DEVELOPMENT OF INVESTMENT CASTING METHOD FOR PRODUCTION OF METAL FOAMS FOR TISSUE ENGINEERING

by

Justin A. Womack

A Thesis Submitted in

Partial Fulfillment of the

Requirements for the Degree of

Master of Science

in Engineering

at

The University of Wisconsin-Milwaukee

August 2019

ABSTRACT

DEVELOPMENT OF INVESTMENT CASTING METHOD FOR PRODUCTION OF METALLIC FOAMS FOR TISSUE ENGINEERING

by

Justin A. Womack

The University of Wisconsin-Milwaukee, 2019
Under the Supervision of Professors Dr. Pradeep Rohatgi and Dr. Benjamin Schultz

Ideal biomaterials for bone tissue regeneration are bone-mimicking structures that present a fully interconnected porous structure, have similar mechanical properties to bone, and exhibits a specific biodegradation behavior that is at the same rate as adjoining cell growth. Metals have high wear resistance, ductility, impact strength, and strain energy absorption capacity compared to other materials, which makes them suitable candidates for tissue engineering scaffolds. Magnesium and zinc are of interest for bone tissue regeneration for their biocompatibility and mechanical properties close to human bone. A newly developed process, presented in this thesis, for the creation of porous magnesium and zinc scaffolds, using rapid prototyping, developing a ceramic mold, and an investment casting procedure, shows promise for the requirements of the scaffold. This process was able to produce zinc scaffolds with pore sizes varying from 1000 μm to 2500 μm. These scaffolds had pore and strut sizes within 5% error of their CAD design. Lastly, the scaffolds produced had mechanical properties within the range of human cancellous bone.

To David Benioff and D.B. Weiss

For reminding me and the world

That if we do not complete our own work

Someone will come along and completely destroy it.

TABLE OF CONTENTS

LIST OF FIGURES

LIST OF TABLES

LIST OF EQUATIONS

LIST OF ABBREVIATIONS

°C – degree Celsius

3D – Three Dimensional

$CaCO_3$ – Calcium Carbonate

CaO – Calcium Oxide

$CaSO_4$ – Calcium Sulfate

EDS – Energy-dispersive X-ray spectroscopy

PLA – Polylactic Acid

PSI – Pound per square inch

SEM – Scanning Electron Microscopy

STL – Stereolithography

TE – Tissue Engineering

TGA – Thermogravimetric Analysis

XRD – X-ray powder diffraction

ACKNOWLEDGEMENTS

Thank you Dr. Benjamin Schultz for your endless patience, advice, and friendship. This project would have been much more unbearable without you as my mentor.

CHAPTER ONE: INTRODUCTION

1.1 Research Goal

The goal of this research was to develop a new process for producing metallic foams, particularly magnesium and zinc metal foams, that overcome many of the setbacks of current methods. We sought to develop an investment casting method that produced metal scaffolds of a desired and controllable pore size for tissue engineering. The casts would be reproductible and cheap with no requirement of harmful solvents or other dangerous methods. This research began by looking for a cheap, easily mendable, sturdy, high temperature enduring, and easily removable. after infiltration of the metal, spacer material. The next step was finding a way to shape this material into a desirable mold for metal melting. The last step was determining the optimal way to remove the mold material without damaging the metal scaffold it held.

1.2 Thesis Organization

This thesis begins with a dedication and acknowledgement to myself for all the hard work, long hours, countless dollars, and bits of my sanity that were put into the completion of the development of this process. The reader will then find the literature review section detailing the background information of bone illness, tissue engineering (TE), TE scaffolds, and why magnesium and zinc are currently being explored for bone regeneration. Next, the most notable, a description of current methods for producing magnesium and zinc scaffolds. To conclude the literature review section, the reader will find the important elements of a TE scaffold and how they relate to the bone regeneration. The next section is the methods section,

detailing the step by step procedure that was created in this thesis—this is the bread and butter of the project. Finally, the results section will investigate the produced foams, examining microscopy, mechanical properties, reactions with the metal and mold material, and how the final metallic scaffold compares to its original CAD design.

CHAPTER TWO: LITERATURE REVIEW

2.1 Background and Importance

Bones, when damaged by illness, stress, or disease, have regenerative properties allowing them to self-heal, with the caveat that only a small fracture exists. However, bone injuries can reach a size where intra-osseous and self-healing will not take place during a patient's lifetime. These size defect injuries often the result from extreme trauma, congenital defects, or cancer resections and therefore can be difficult to impossible to treat by conventional methods[1]. The gold standard current method, the autograph, involves using a three-dimensional (3d) bone graft substitute taken from a different part of the patient's body to replace and treat the loss or injury of the bone. However, the use of a bone graft substitute is limited by harvesting difficulties, donor site morbidity, and the clinicians' ability to contour delicate 3d shapes[2]. Bone tissue engineering (TE) is an emerging field that will treat critical size bone defects where the conventional current gold standard fails. The goal of bone tissue engineering is to regrow and repair, without the use of a bone graft substitute, bone tissues damaged beyond the natural healing capacity of the human body. It will be done using a combination of knowledge from materials science, biomechanics, molecular development biology, cell biology, and biomedical engineering[3]. In general, three elements are necessary to successfully engineer the biological tissues of a bone. The first required element are the cells that differentiate and form bone tissue (osteogenic cells) along with the proper signaling molecules to induce differentiation. The second element is a biocompatible, porous scaffold conducive to normal cell functions that will allow the cells and tissue to form on and

throughout its matrix. Lastly, there must be proper signaling and biomolecules to induce differentiation and sustain the growing of living tissue [4]. The overall process can be seen in Figure 1, where a scaffold with cells and biomolecules is placed into a wound and grows to form a new bone.

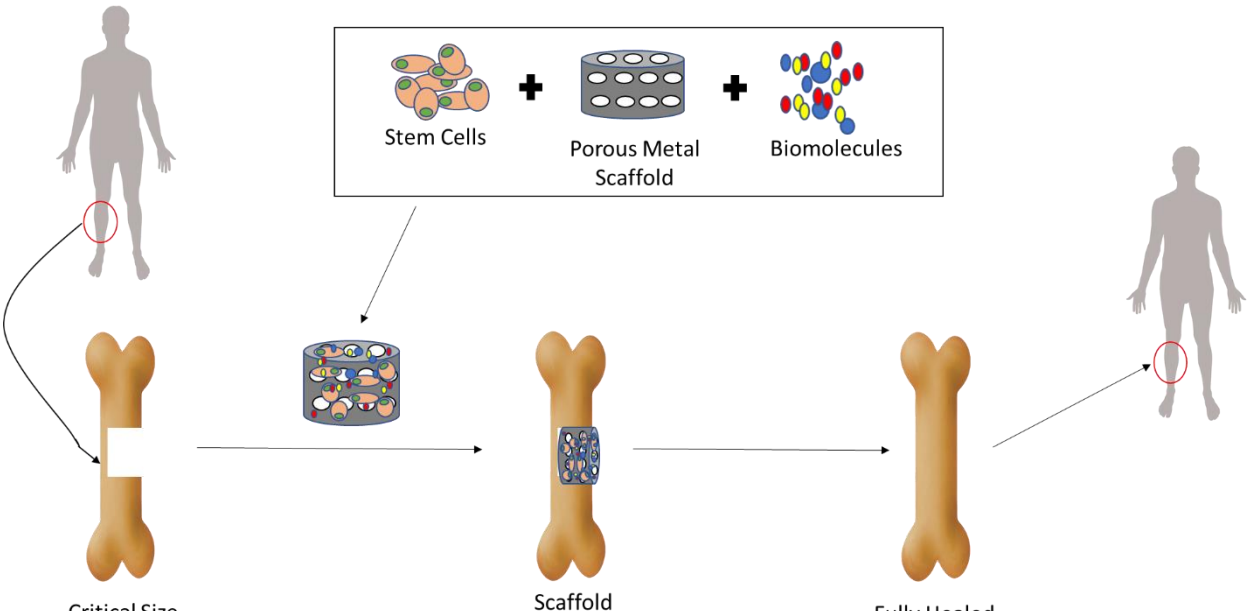

Figure 1: Overall bone tissue engineering process.

A tissue engineering scaffold is a three-dimensional biocompatible structure that when placed into a patient provides mechanical support, a template for cell attachment, and stimulates tissue formation by mimicking properties of the extracellular matrix[5].

A biocompatible scaffold for bone tissue engineering requires the building biomaterials to be osteoinductive, porous, and mechanically compatible with native bone. In addition to these properties, a biocompatible scaffold must integrate with the surrounding native tissues and provide anchorage sites and structural guidance to osteogenic cells. Thus the

scaffold creates an interface that responds to physiologic and mechanical change within an in vivo environment[1].

To summarize, TE scaffolds are required to perform each of the following six functions:

1) Deliver progenitor cells or facilitate host cell recruitment
2) Deliver important signaling molecules in a temporally and spatially controlled manner
3) Promote vascularization and tissue growth
4) Properly fit the shape of the anatomical defect
5) Provide initial plasticity while maintaining load bearing stability
6) Degrade into a biocompatible byproduct at a rate that matches new tissue growth formation

2.2 Bone Tissue Engineering Scaffold Materials

The current, commonly researched scaffolds are natural and synthetic polymers, ceramics, and composites of the two. However, these types of scaffolds lack the load bearing strength necessary for placement in hard tissue. Additionally, many polymers break down into toxic components and can undergo a bulk erosion process causing the scaffold to fail prematurely. The abrupt release of these acidic degradation products can cause a strong inflammatory response in surrounding tissue. Other problems with ceramic scaffolds include concern over their resorption, porosity , and their natural brittleness leading them to be undesirable for load bearing bone substitute applications[6]. For the reasons stated above, other materials are being explored for hard tissue engineering, particularly of the metallic variety.

Metals have high wear resistance, ductility, impact strength, and the capacity to absorb high strain energy compared to other materials, which has made them suitable candidates for many orthopedic biomedical applications such as fixation devices for joint replacement, bone plates, and screws, dental implants, suture wires, and coronary stents. Traditionally, corrosion-resistant metals, such as stainless steel, cobalt-chromium alloys, and titanium alloys, have been used for medical implants[7]. However, these metals lack biocompatibility, so focus has shifted towards finding alternatives that remain comparable in strength and durability while increasing suitability with the human body. Because of this, the focus of the medical industry has shifted from using permanent implant devices to using biodegradable materials for implantation, helping to avoid some drawbacks of permanent implantation including permanent physical irritation, chronic inflammatory local reactions, mismatches in mechanical behavior between implanted and non-implanted areas, and the inability to adapt to the growth of young patients[8].

Metal foams are composites of metal that incorporate a porous matrix into their structure, leading to a low density without large decreases in mechanical properties[9]. They retain many of the strong mechanical properties of a solid metal, including good energy absorption and high strength. Metal foams have the additional advantage of being ultralight with a higher compression strength compared to the solid material while introducing characteristics of permeability, controlled pore structure and size, thermal shock resistance, and acoustic, vibration, and shock dampening[10]–[12]. Additionally, metal foams have the porous space necessary to seed cells and facilitate their growth. Lastly, the biocompatible, porous metallic

foams that are being investigated can degrade in the body, which bypasses the need for a removal surgery and avoids the drawback of permanently implanted metals orthopedics.

2.2.1 Magnesium as a Tissue Engineering Scaffold

Magnesium composites are of interest for bone engineering scaffolds as they have been shown to be fully bioresorbable, have mechanical properties aligned to bone, induce no inflammatory or systemic response, are osteoconductive, and encourage bone growth when undergoing degradation[6], [13]. Magnesium alloys have a specific strength and elastic modulus close to natural bone, allowing it to avoid a stress shielding effect [14][15]. However, magnesium has a high corrosion rate resulting in the rapid release of degradation products in the body [13], [16]. Another cause for mass loss of magnesium and its structural integrity is the embrittlement of the metal itself due to the production of hydrogen gas at the site of degradation, which can lead to bits of metal 'falling off' in solution[17]. In addition, studies have shown that the corrosion of magnesium and its alloys can coat the scaffold with a surface film that hinders the cell growth of the developing tissue[5]. Interestingly, other studies, have shown that the degradation of magnesium leads to higher bone cell activation in the surrounding tissue[13]. The corrosion of magnesium does not require that bare metal surface to be present to the surrounding environment, meaning any tissue or cells in the immediate vicinity of the magnesium based implant will be in intimate contact with the dissolution magnesium ions, encouraging bone growth even if the surface of the magnesium is coated with a substance that helps encourage cell attachment, growth, and proliferation [5]. Magnesium metallic foams are an emerging option for a biocompatible scaffold since the porous structure can resemble that

of bone and the foam possess all the before mentioned positive attributes of magnesium composites for bone tissue engineering.

2.2.2 Zinc as a Tissue Engineering Scaffold

Zinc is an emerging metal that is being explored for its possible potential in tissue engineering. Compared with magnesium, zinc has a better corrosion resistance in aqueous solutions and is not connected to hydrogen gas evolution [18]. Furthermore, zinc is a highly essential element for humans and plays an important role in many physiological functions (such as normal growth, immune functions, protein and DNA synthesis, and wound healing) [19], [20]. Zinc also regulates bone homeostasis, accelerates bone density and remodeling, and enhances bone resorption inhibition[21]. However, very few studies have been performed with zinc scaffolds as zinc tends to lack the mechanical properties necessary of a bone scaffold. Alloying zinc is a way to improve its mechanical properties, has a positive effect on the degradation behavior, and displays *in vitro* cell proliferation and antibacterial behavior [22], [23]. Despite zinc's drawbacks and advantages, more studies are needed to determine its potential as a tissue engineering scaffold.

2.3 Current Methods of Producing Magnesium Foams

Magnesium foams have been studied extensively and many different methods have been created for their production. However, magnesium is a difficult metal to process and shape into an ordered porous structure. It poses many problems, most notable is magnesium's very high reactivity to other elements. Another problem that arises is the ability to consistently form a replicable porous structure of the exact same design. Lastly, many processes involve

dangerous procedures including bone burning solvents and experimental setups that can be hazardous, such as trying to 3D print magnesium powder. Regardless, magnesium scaffolds have been produced many ways in the past with the most popular routes being the titanium wire space holder method [18], negative salt pattern molding[19], powder metallurgy[20], [21], hydrogen injection [22], and laser perforation[6].

2.3.1 Synthesis of Porous Magnesium Scaffolds: Space Holder Method

The space holder method is any method that relies on the addition of temporary particles to metallic matrix that hold the space for future pores. In this method, space-holding particles are usually mixed and compacted together with metallic matrix powder particles and then removed before or during sintering, leaving new pores behind in the matrix. A number of spaceholder molecules have been created including carbamide, ammonium hydrogen carbonate, sodium chloride, starch, saccharose, polymethy-methacrylate, and paraformaldehyde[23].

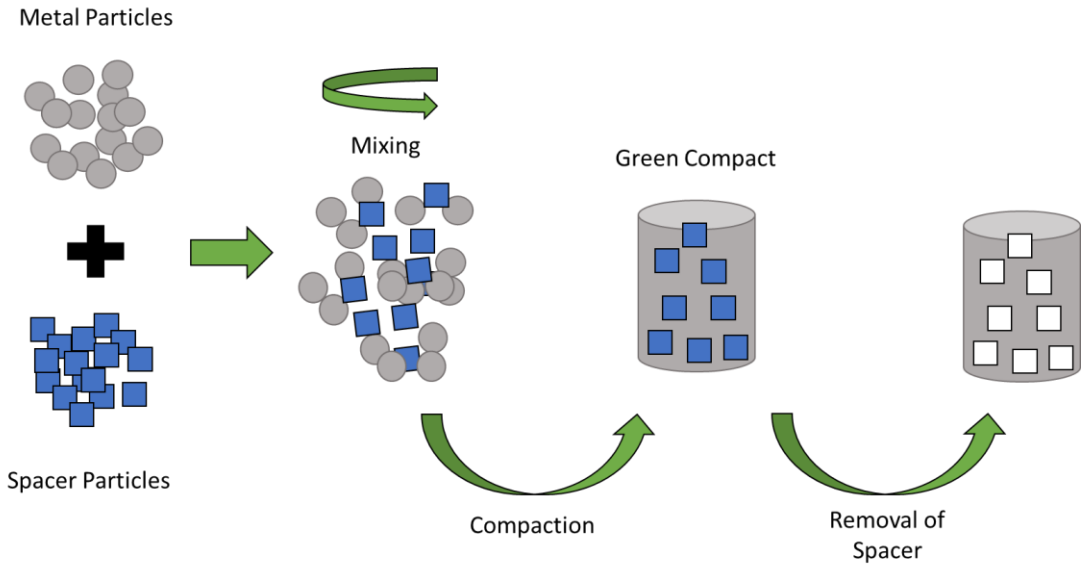

Figure 2: Overview of spacer method.

Currently, heat treatment and liquid leaching are the two commonly used techniques for removing a space holder to create a porous structure. Removal by heat treatment is based on the thermal decomposition and evaporation of space holding material. At the selected removal temperature, the space holder evaporates and escapes from the scaffold with the flushing gas of the furnace[24], [25]. In liquid leaching, the scaffold is immersed in a liquid to allow the dissolution and leaching of the space holder. The leaching medium is dependent on the space holder material. The most common leaching media used for sodium chloride, carbamide, saccharose, and corn starch dextrin space holders is water[26], [27]. Other medias used include, NaOH, hydrochloric acid, hydrofluoric acid, acetic acid, and ethanol[28], [29].

One of the more recent, promising space holder methods involve using titanium wire as the space holder. This method involves creating a 3D entangled titanium wire material and then infiltrating it with magnesium melts. The titanium wires are then removed by a hydrofluoric (HF) solution leaving an open-porous magnesium scaffold. This method can easily control the pore size and porosity as well as regulate the mechanical properties to be within the range of human bone by changing the orientation of the pores. However, it requires expensive machinery and the use of dangerous solvents to remove the space holder. Regardless, this method has been used to produce high porosity scaffolds (up to 70%) with interconnected pores of size 200-500um[2].

2.3.2 Synthesis of Porous Magnesium Scaffolds: Laser Perforation

Laser perforation is a technique for making porous magnesium scaffolds that does not involve the use of a space holder. In this process, pure magnesium ingots are treated in a multifunction

laser processing machine. This machine uses lasers to create interconnected and homogenous pores with round and honeycomb like structure. This method also allows for control over the structure, size, and shape of the pores[30]. This method looks promising, but more studies need to be done to confirm its repeatability. In addition, it requires expensive machinery that makes it difficult to mass produce and test these scaffolds.

2.3.3 Recent Advances in the Production of Porous Magnesium Scaffolds

Two newer methods of producing magnesium foams are of interest in the recent years. The first, the fiber deposition hot pressing method, involves creating a network structured unit of magnesium fibers layered in graphite dies, then hot pressing the unit to create porous mg scaffolds [15]. This method was able to produce magnesium scaffolds with mechanical properties similar to bone: a compressive strength ranging from 11.1- 30.3 MPa and a young's modulus of 0.10-0.37 GPa [15]. Since the mechanical properties of porous magnesium fall in the range of cancellous bone, it makes this material a suitable option for bone tissue regenerative scaffolds. The second method is a rapid prototyping method, known as selective laser melting (SLM), to produce magnesium foams. This method is of interest because it can 3d print magnesium scaffolds of replicable structure, an impressive but dangerous feat. Additive manufacturing methods for creating magnesium have been avoided in the past as magnesium is highly flammable and could have the potential for a dust explosion. Another drawback of this method is it requires the use of a specific alloy of magnesium and has not been expanded on to other alloys or pure magnesium. Regardless, porous magnesium scaffolds produced by SLM, using a diamond lattice unit cell, created a scaffold with a porosity of 64% and a modulus of 0.7

GPa [31]. This method could prove to be a useful way to produce magnesium scaffolds if safety concerns can be alleviated.

2.4 Current Methods for Producing Zinc Scaffolds

Problems emerge when zinc scaffolds are attempted to be produced by conventional methods that are used to produce other porous metal scaffolds. The application of the space holder technique for zinc-based materials is difficult because of the low melting point of zinc (420 °C) and its reactivity with ammonium, which is formed by the decomposition of low-temperature space holder materials, such as ammonium bicarbonate. Similarly, fabrication of porous zinc by the additive manufacturing techniques may be difficult because of the low melting and boiling point of zinc (420°C and 907 °C).

Regardless, in the recent years, porous zinc scaffolds have been produced in a few ways. The first method was to combine pressure infiltration with a sodium chloride (NaCl) template. In this method, NaCl serves as a mold that the zinc is melted into and then removal of the mold takes place. While the zinc scaffolds produced by this method had 54-71% porosity, they lacked mechanical properties necessary for a bone scaffold. However, their properties show that they are still suitable for non-load bearing or low load bearing applications. These scaffolds were also found to dissolve at a rate tolerable by the human body[32]. Another group has produced zinc scaffolds through plasma spark sintering that possess properties similar to human trabecular bone, but have yet to test for toxicity and biocompatibility of these scaffolds[33]. Additionally, the alloying of Zinc with 3% Copper using pressure infiltration and NaCl templates has created scaffolds with higher mechanical properties but has significantly increased the rate

of degradation of the scaffolds, removing one of their more attractive traits for tissue engineering[34].

2.5 Important Physical Properties of Porous Metallic Scaffolds

Morphologically, two types of bone make up the overall bone. The first, compact, or cortical bone, is the extremely hard, dense outer layer of bone and accounts for 80% of overall bone mass[1]. The second, cancellous bone, fills the inter cavity of long bones and is the location of metabolic responses in the bone. Cancellous bone is spongy in nature having 50-90% porosity by volume while cortical bone has less than 10% volume porosity[35]. The spongy nature of cancellous bone leads to it having a low density and strength but has a very high surface area compared to cortical bone's hard nature.

The bone is comprised of two types of cells: osteoblasts and osteoclasts. The former are the cells that responsible for new bone formation while the latter are responsible for resorption of old bone[35]. Bone is also highly vascularized, meaning that a bone scaffold must be capable of angiogenesis otherwise oxygen and nutrients will have trouble reaching growing cells. This improper vascularization leads to oxygen and nutrient deficiency which may result in cell death[36].

2.5.1 Mechanical Strength

It is ideal for the bone scaffold to have mechanical strength similar to that of bone. If the scaffold lacks mechanical strength, then the scaffold can fail to support the surrounding bone tissue. If the scaffold's mechanical strength is to much higher than the surrounding bone a

stress shielding effect will occur. Stress shielding refers to the reduction in mechanical stress in the bones adjacent to the implanted scaffold. This weakening of the surrounding bone tissue can lead to loss of bone stock and can cause loosening of the implanted scaffold [37]. The lack of mechanical strength is one of the challenges that nonmetallic scaffolds face. Most metallic scaffolds have mechanical properties that are too high and will cause a stress shield effect, however, magnesium alloys have a specific strength and elastic modulus closer to natural bone [14][15].

Compressive strength is the property that is most often used to characterize the mechanical behavior of a bone scaffold. The compressive strength of human cortical bone ranges between 0.2 to 80 MPa, with tensile strengths ranging from 90-190 MPa [14], [38]. The other commonly used property is the young's modulus, which 0.01-2 GPa is the range for bone [39][40]. Magnesium alloys are 3-16 times stronger than biopolymers and, at the same time, they are more ductile reducing the chance of the device fracturing throughout the implantation process. Titanium is a commonly used metal in surgical implants. However, its modulus (110-117 GPa) is much too high to be used as a bone engineering scaffold and is often seen producing a stress shear effect. Zhang et al produced magnesium scaffolds with mechanical properties similar to bone: a compressive strength ranging from 11.1- 30.3 MPa and a young's modulus of 0.10-0.37 GPa [41]. Since the mechanical properties of porous magnesium fall in the range of cancellous bone, it makes this material a suitable option for bone tissue regenerative scaffolds.

Table 1: Compressive property of bone.

	Density (g/cm^3)	Compressive Strength (MPa)	Stiffness (GPa)	Fracture Toughness ($MPam^{1/2}$)	Microhardness (GPa)
Cortical Bone	1.7 - 2.0	130 - 180	7-30	2 - 12	0.62 - 0.74
Cancellous Bone	0.03 - 0.12	0.1 - 16	0.05 - 0.5	-	0.52 - 0.74

2.5.2 Degradation

Magnesium is a biodegradable metal and will degrade slowly in the body. This is ideal since a biodegradable metal scaffold should disappear entirely upon fulfilling its job of supporting the tissue regeneration. This is ideal as it require no surgical operation for implant removal[42]. Ideally, the produced magnesium scaffold would need to have a low in vivo corrosion rate and a high strength. However, the main challenge for employing Mg and its alloy as an implant is its high corrosion rate resulting in the rapid release of degradation products in the body[13]. In addition, studies have shown that the corrosion of magnesium and its alloys can coat the scaffold with a surface film that hinders the cell growth of the developing tissue[5].

An aspect of magnesium degradation that is especially relevant to biological systems is oxidation-reduction reaction that occurs between water and magnesium. The standard electric potential of magnesium is much lower than that of water, and thus magnesium can easily be oxidized as it gives up its electrons and reduces water to hydrogen gas and hydroxide. This is also the cause of the hydrogen gas buildup that can be seen in vivo when magnesium scaffolds

degrade too quickly. The increase in the local hydroxide ion concentration leads to an increase in pH around the site of degradation. Magnesium leaves the bulk of the metal and dissolves in the solution as magnesium ions (Mg^{2+}) because of the degradation reaction, resulting in mass loss of medical implants[16]. Another cause for mass loss of magnesium and its structural integrity is the embrittlement of the metal itself due to the production of hydrogen gas at the site of degradation, which can lead to bits of metal 'falling off' in solution[17].

Physiological salt ions in body fluids can aggressively attack magnesium and accelerate its degradation. Magnesium degradation in physiological fluids mostly occurs through Equation 1 below[43], [44]. In aqueous environments, a degradation layer composed of $Mg(OH)_2$ forms on the surface of magnesium through the second reaction in Equation 1. The degradation layer only provides limited protection to magnesium from subsequent degradation due to its loose and porous microstructure[17].

$$Mg + 2H_2O \rightarrow Mg^{2+} + 2OH^- + H_2$$

$$Mg^{2+} + 2OH^- \leftrightarrow Mg(OH)_2$$

Equation 1: Reaction of the degradation of Magnesium in aqueous solution.

The creation of magnesium oxide on the surface of the scaffold creates another problem in the body and that is the reaction between magnesium hydroxide and chlorine ions from the tissue fluid. This leads to the production of magnesium chloride with is a high water soluble compound that can degrade with passing water molecules[45].

The degradation of magnesium leads to higher bone cell activation in the surrounding tissue[13]. The corrosion of magnesium does not require that bare metal surface to be present

to the surrounding environment, meaning any tissue or cells in the immediate vicinity of the magnesium based implant will be in intimate contact with the dissolution magnesium ions, encouraging bone growth[5].

2.5.3 Coatings to Fight Degradation

The major drawback preventing magnesium from being applicable as a tissue engineering scaffold is its rapid degradation. This early degradation rate results in a weakening of the mechanical strength of the scaffold[44]. Generally, there are two possibly ways to improve corrosion behavior of Mg and Mg alloys. The first is to tailor the composition and microstructure, including grain size and texture. The second is to carry out surface treatments or form coatings to provide protective layers. Coatings can be divided into two classes: conversion and deposited coatings. Conversion coatings are formed by a specific reaction between the base metal and the environment. The most notable case of this is the growing of an oxide layer on the base metal. Deposited coatings are mostly organic base materials that are placed on the surface of the base metal to form a resistive coating. Ideally, coatings can provide more functionality than corrosion resistance. They can increase osseointegration, bioactivity, antibiotic ability, or local drug delivery[46].

Polycaprolactone (PCL) is a popular FDA approved polymeric coating that shows promise to help control the degradation rate of magnesium. Yazdimamaghani et al has performed experiments with PCL on magnesium scaffolds. They found that magnesium coated in 3% and 6% PCL only experienced 36% and 23% degradation after 72 hrs compared to 100% degradation by magnesium scaffolds without coating. Another popular coating that has been studied is

beta-tricalcium phosphate (BTCP). Calcium phosphate is a chemical that is found in bone and BTCP is a derivative that possess high chemical stability, relatively high mechanical strength and a favorable biodegradation rate. Magnesium scaffolds coated with BTCP show slower degradation as well as increases in cell adheration and proliferation compared to a magnesium scaffold with no coating[6].

Fluoride coating has emerged as a promising deposition coating that has been applied to magnesium and its alloys by multiple authors. This coating takes on the form of MgF_2. The results demonstrate that fluoride can be used to reduce the initial corrosion rates in vitro and in vivo[47][48]. Furthermore, fluoride has been shown to have beneficial effects bone formation in vivo[30]. Post treatment with alkali-heat treatment has also been showed to slow degradation[6].

2.5.4 Porosity and Pore Size

Porosity is the controlling variable of a bone engineering scaffold. The pores are necessary for bone tissue formation because they allow migration and proliferation of osteoblasts as well as the space needed for vascularization. This is likely due to the larger surface area that results in a higher ion exchange and bone inducing factor adsorption [49]. In addition, the porous surface improves mechanical interlocking between the scaffold and the surrounding natural bone, a process known as osseointegration [50]. High porosity and large pores enhance bone ingrowth and osteointegration of the scaffold after surgery. However, high porosity is related to weaker mechanical properties and faster degradation [49][51]. Increasing porosity results in the decrease of compression strength, yield strength, and Young's modulus. Also, a higher porosity

will lead to a quicker breakdown of these two properties. As the porous structure degrades it will get mechanically weaker. Too high of a porosity will lead to a quick degradation, leading to a quick spike in pH and the formation of a hydrogen bubble near the implanted scaffold [51]. This could lead near nearby cell death of surrounding tissues and rejection of the porous scaffold.

In addition to porosity, the pore size is also a crucial morphological property of a porous scaffold for bone regeneration. While no optimal pore size has been determined, there is agreement among experts that the scaffold should exhibit porosity in excess of 50% with a minimum pore size of 100 µm. The optimal pore size is still debated though. A study by Meng-qi Cheng et al found that pore sizes around 1000 µm favor osteoblast phenotype expression, while a pore size of 500 µm allows for more bone formation[51]. A different study determined 325 µm to the optimal pore size. However, this study demonstrated that a high specific surface area was more important that pore size for cell attachment to the scaffold for the first 48 hours. After 48 hours, a higher mean pore size takes a dominant effect on cell attachment and proliferation[52]. Many studies have shown that better osteogenesis occurs with pores > 300 µm[47], [52],[49], [51]. The upper limit on pore size is the issue being debated. Relatively larger pores favor direct osteogenesis, since they allow vascularization and high oxygenation, while smaller pores result in osteochondral ossification[30]. It has been suggested that the ideal scaffold should present pores in both sizes, however there is a lack of current research on this subject.

Table 2: Pore size distribution for an ideal scaffold in bone tissue engineering [53].

Pore Size (μm)	Biological Function
< 1	Protein interaction, responsible for bioactivity
1-20	Cell attachment, their orientation of cellular growth
100-1000	Cellular growth and bone ingrowth
> 1000	Shape and functionality of implant

A difficulty in scaffold design has been choosing a design parameter that completely and accurately characterizes the effect of the scaffolds pore architecture on mass transport and ultimately on bone growth. Because of the inconclusive results of an optimal pore size, it has recently been proposed that permeability, instead of pore size, of the scaffold should be tested parameter to determine a scaffolds ability to regrow bone. Permeability is variable that measures the ability of a porous medium to conduct fluid flow and is dependent on porosity, pore size, orientation, tortuosity and interconnectivity[52]. A low permeability has been shown to induce cartilage formation instead of bone while a higher permeability is believed to improve bone growth. Permeability and flow in the porous scaffold can be described by Darcy's law:

$$\boldsymbol{q} = -\frac{\boldsymbol{K}}{\boldsymbol{\mu}} \cdot \boldsymbol{\nabla P}$$

Equation 2: Darcy's Law to determine the permeability of a porous structure.

where q is the Darcy flux vector, ∇P the pressure gradient vector, μ the fluid viscosity, and K is the permeability matrix.

2.6 Summary of Literature on Metal Scaffolds for Bone Regeneration

The complexity of biological processes currently dwarfs the sophistication of the current generation of therapy intended to direct, accelerate, repair, and regenerate bone tissues. There are increasing, urgent demands to repair bone defects, and damages caused from bone fractures, bone cancer, bone infections, and other serious bone injuries. Convention repair methods involving the use of various biomedical bone implants or conventional tissue replacement (autografts and allografts) cannot meet the quantity or necessary performance required. Bone tissue engineering is an emerging field to replace these conventional methods. Bone tissue engineering makes use of a porous scaffold to provide the required pathways for cells to grow, proliferate, and differentiate. In addition, the architecture of the scaffold defines the final structure of the newly formed bone. Magnesium based scaffolds are emerging as a promising material to design a bone scaffold. Magnesium is fully bioresorbable, has mechanical properties aligned to bone, induces no inflammatory or systemic response, is osteoconductive, and encourages bone growth when undergoing degradation. Previous studies have shown that degradation of Mg scaffolds was too fast to match the growth of new tissue which continues to be a problem moving forward with magnesium scaffold design. This fast degradation leads to low rates of hydrogen gas being formed near the site of scaffold which if accumulated too fast can lead to necrosis of nearby cells. A bone engineering scaffold can be coated with certain biocompatible polymers or chemicals to help reduce their quick rate of degradation. Specific coatings have been showed to decrease the degradation rate of scaffolds as well as increase cell adhesion and gene expression of the growing tissue. Scaffold design is dependent on porosity and pore size and no optimal value for these terms has been determined. It has been

determined that an increased porosity and pore size facilitate bone ingrowth but this increased porosity results in a reduction in mechanical properties that compromises the structural integrity of the scaffold. The ultimate surgical success of implanted mg will depend on i) a controllable and predictable degradation process; ii) low rates of hydrogen gas evolution during dissolution; (iii) retention of mechanical properties); and (iv) indeed most principally, satisfactory biocompatibility and osteoconductivity [5].

CHAPTER THREE: EXPERIMENTAL METHODS AND PROCEDURE

The overall investment casting procedure can be seen below in Figure 3. The procedure starts with the computer aided design (CAD) of the engineered scaffold in Creo Parametric. The part is then created by rapid prototyping using the thermoplastic Polylatic Acid (PLA). A liquid, ceramic mold material is then prepared and is infiltrated into the pores of the engineered PLA part. A burnout of the overall mold is performed and then the selected metal is infiltrated into the mold. The mold material is then dissolved out of the metal scaffold, leaving the metal replicate of the 3d printed part.

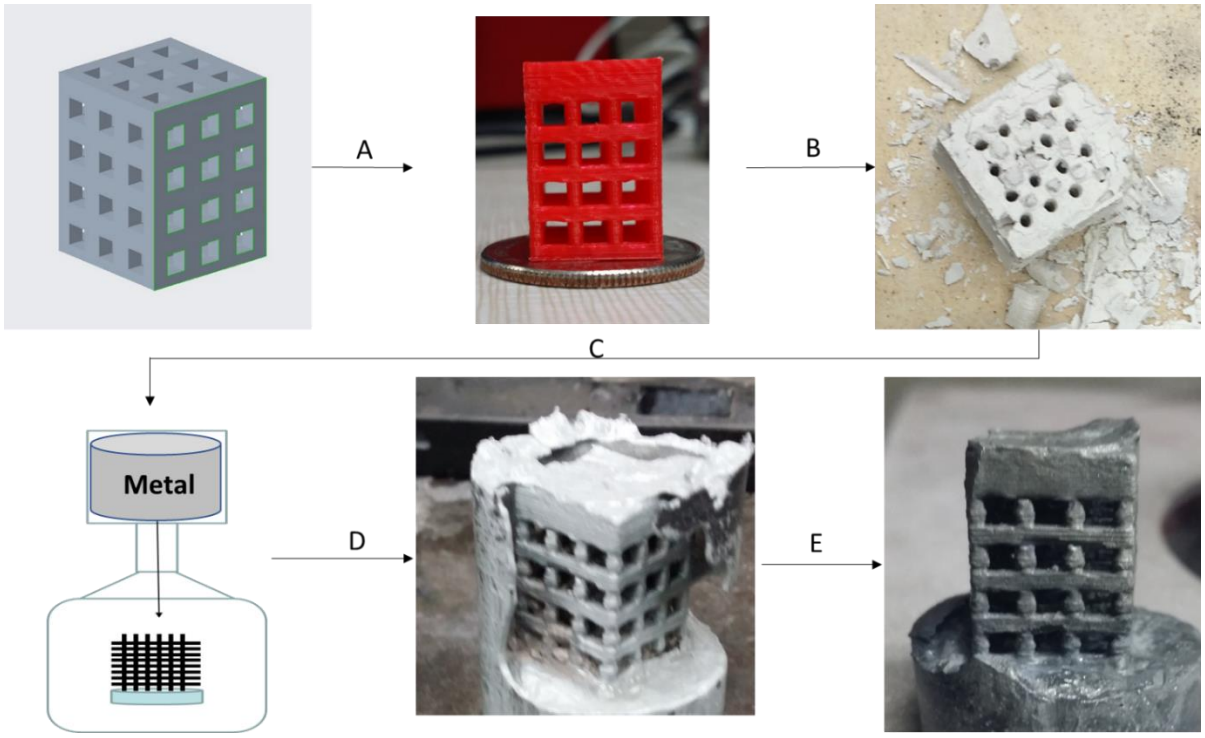

Figure 3: Description of the overall process beginning with the designing of the model in Creo Parametric. (A) CAD designed model 3D printed in PLA. (B) Infiltration of PLA with ceramic paste and subsequent burnout of PLA and sintering of ceramic. (C) Infiltration of ceramic with metal. (D) Removal of ceramic spacer material. (E) Removal of excess metal from casting procedure.

3.1 Design of Model in Creo Parametric

The model is designed using the lattice function in Creo Parametric. This was found to be the easiest way to design the scaffold without taxing the random access memory (RAM) of the computer operating system. Other methods, such as creating a unit cell that is repeatedly copied and pasted or using the pattern function, were found to be to computationally taxing on the operating system causing a crash or freeze of the program. As the lattice function is not typical used to design tissue engineering scaffold and as there are no publicized accounts on how to use this function to do so, the procedure will be documented in this thesis. The following is a step by step procedure of designing a scaffold made up of unit cube:

1. Open Creo Parametric and create a solid part using the default template. This template uses inches but the unit is unimportant as saving the file as a '.stl' will make the file dimensionless.

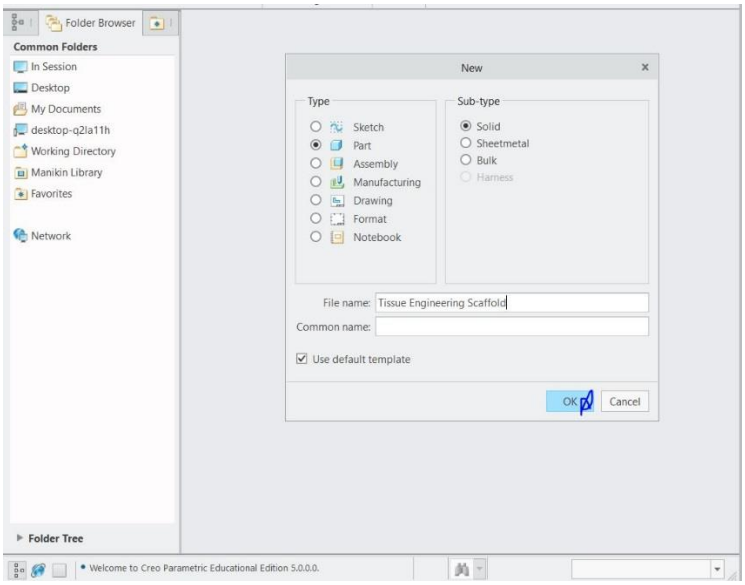

Figure 4: Starting the design of a 3d tissue engineering scaffold in Creo Parametric.

2. Create a sketch of the desired structure in the x and y plane. In this example, a square of 15mm by 15mm is sketched to be used as the base of the scaffold. Select the front plane and then click the sketch button in the model tab. Select the square function, draw, and size it to the desired units (in this case 15mm x 15mm).

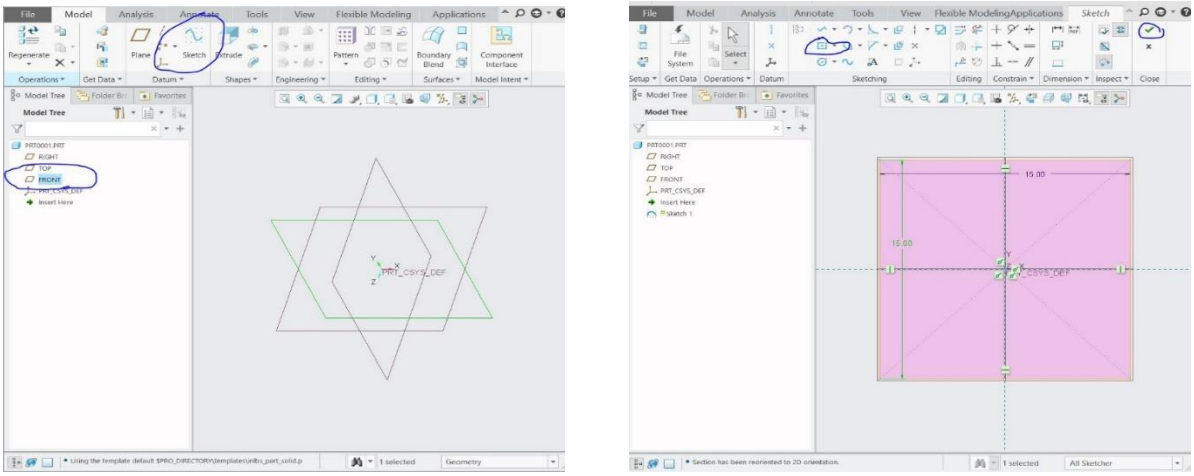

Figure 5: Sketching a square base in Creo Parametric for design of tissue engineering scaffold

3. Extrude the structure to create the necessary height by clicking the extrude button (next to sketch) and selecting the desired height. In this case, a height of 17mm is selected.

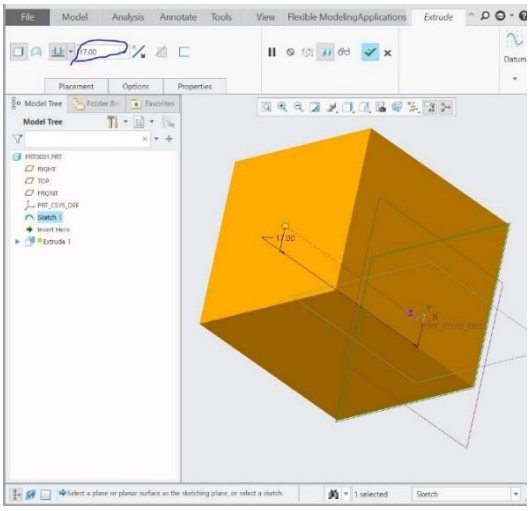

Figure 6: Extruding a rectangle from sketch in Creo Parametric to be latticed into a porous solid

4. The next step is to create the porous structure. To create the lattice object, click the lattice function under the engineering tab. Now in the lattice table, click references and then click the convert solid box. This will show the current unit cell on the model.

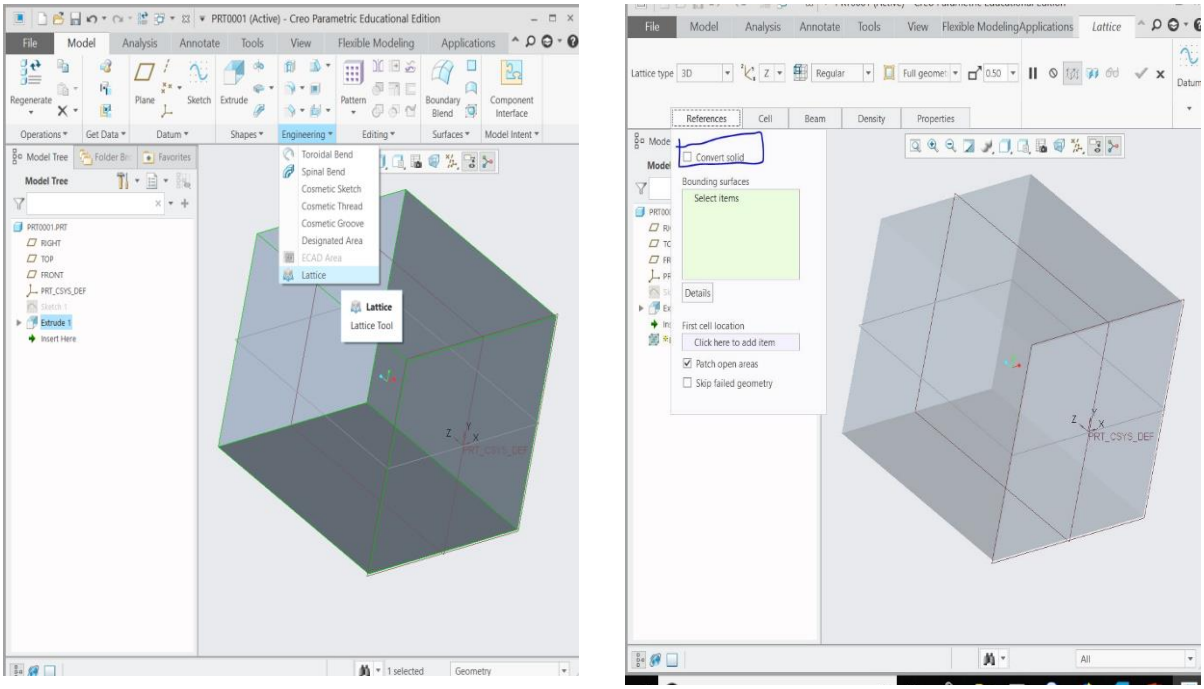

Figure 7: Using the lattice function in Creo Parametric to convert a solid rectangle to a porous object.

5. The next step is to edit the size, shape, and type of beams in the unit cell that will make up the tissue engineering scaffold. Click on the cell tab and begin by selecting the cell shape. In this example, we will select square. The cell size will change the dimensions of the unit cell in the desired direction. In this example, change all three orientations to be 3. Next, unclick the boxes for angular beams, inner horizontal beams, and outer horizontal beams. This creates a clear square unit cell without all the crossbeams.

Note: The lattice function will often create an object that has overhanging beams and

looks messy and will add parts to the structure that are unnecessary. These overhangs can be removed with a simple knowledge of Creo Parametric by selecting the desired face, sketching over them, extruding to remove the material. However, the user can check the box to remove dangling beams that will remove these overhangs or design the model to exact specifications to avoid the dangling beams. While removing the dangling beams works well for some models, it requires more operating power than most standard computers have and will freeze the program. Because of this, the box to remove dangling beams is not recommended to be used without more than 16gb of RAM.

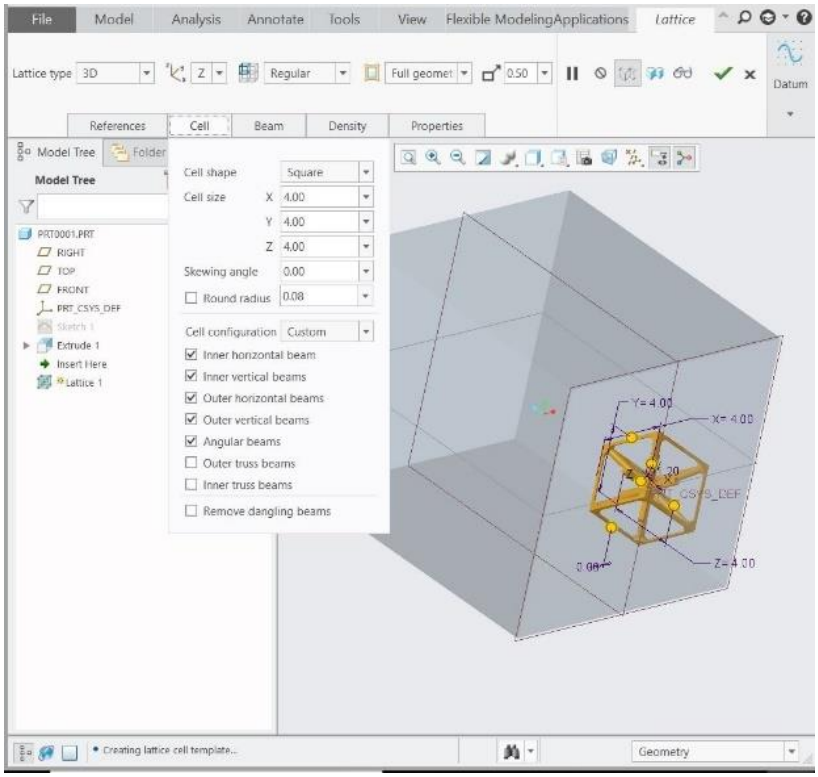

Figure 8: Choosing lattice size and shape for TE scaffold in Creo Parametic

6. Next, the beam size will be chosen. This will determine the size of the metal struts that are created while step 5 was used to create the pore sizes. Click the beam tab and select the cross section type. There are three choices (square, circle, hex) and determine what shape each strut is in. Click square for this example. Then enter the desired strut size into the 'cross section size' box. The example uses a cross section size of 1.50. The ball diameter tab will place a circular ball on all the points where two struts met. Leave this box unchecked. Click the green check mark and the final lattice structure will be created. The icon to the left of the green check mark (the eyeglasses icon) will show the final view of the lattice structure but will not finalize it.

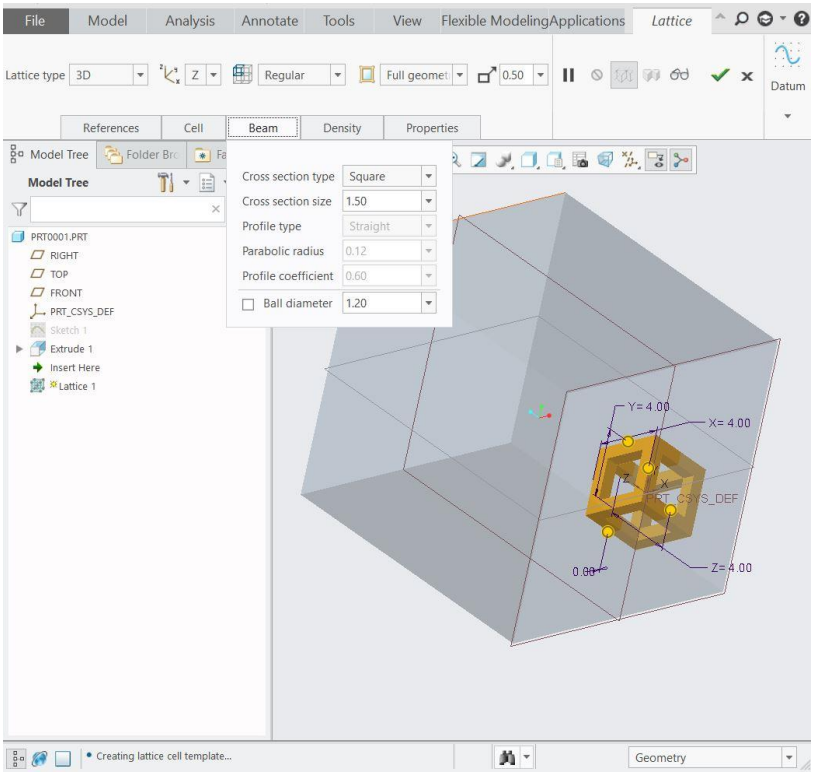

Figure 9: Creating beam size of TE scaffold and effectively choosing the pore size

7. The final designed lattice structure is shown in the below figure. Finally, we want to save this figure. Click File→Save as Copy. Then save the file in the desired directory. It is recommended to save the scaffold as both a '.part' and '.stl'. The first of which will allow the file to be reopened and edited in Creo Parametric and the latter is the needed format required for most 3D printers. This example is a simple cube example, but much more complex structures can be created by choosing a different unit cell shape and by adding crossbeams.

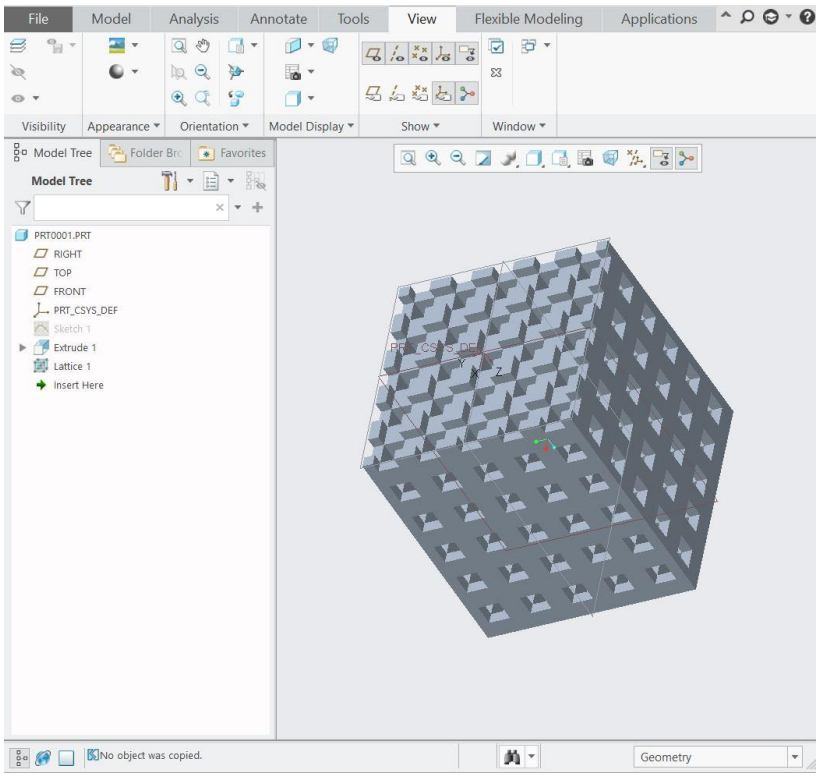

Figure 10: Image of Final TE Scaffold using a unit cube for its lattice structure.

There is an option in the references tab in the lattice function to select the first cell location. This lets one move the first cell to any location that has a created coordinate system. This can be used to bypass the program starting all unit cells in the center of the object if the user wants to use that option.

3.2 Rapid Prototyping of designed models in PLA

All TE scaffolds were 3D printed in clear colored PLA manufactured by Solutech by providing a stereolithography (stl) file to the proper slicing software for the proper printer. Two printers were used for this project: a Creality CR-10 and a Hyrel System 30M. For the Creality CR-10, Cura was used as the slicing software and scaffolds were printed at the following parameters:

Layer Height: 0.1 mm
Infill: 20% (no infill should actually be required for scaffold printing)
Printing Temperature: 200 °C
Build Plate Temperature: 60 °C
Wall thickness: 0.8 mm
Print Speed: 60 mm/s
Fan Speed: 100%

For the Hyrel System 30M printer, slic3r was used for the slicing software under the same parameters as Cura and repretrel was used as the printing GUI for the system. The difference

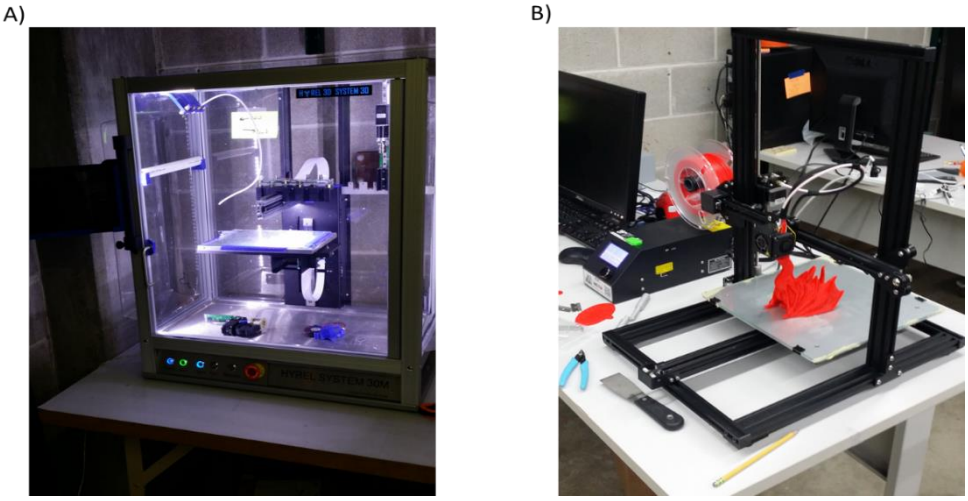

Figure 11: Image of the two different printers used to produce the plastic TE scaffolds. (A) Hyrel System 30M. (B) Creality CR-10.

in slicing software arises because of the programming of the Hyrel 30M printer requires the use of repretrel and slic3r.

3.3 Composition and Design of Ceramic Molds

3.3.1 Calcium Carbonate Mold

Two different paste compositions have been used for this experiment that differ on their choice of binder material. The Table below shows both final paste compositions:

Table 3: Composition of calcium carbonate ceramic pastes

Materials	Paste 1	Paste 2
Calcium Carbonate	100g	100g
Guar Gum	0.30g	0.3g
Sodium Silicate	-	8g
Darvan C-N	2ml	2ml
Deionized Water	36ml	36ml
Graphene Powder	0.010g	0.010g

Two different ceramic paste compositions were chosen for their different properties. Calcium Carbonate, manufactured from North Mountain Supply, was used as the ceramic base of the paste. Laboratory grade guar gum powder, manufactured from Aqua Solutions Inc., was used as a binder for the pastes. Sodium Silicate, manufactured by MCB Reagents, is a high-temperature binder that adds support to the final mold structure. However, it does not burn out during the sintering process of the ceramic mold and proves to be difficult to remove from the final product after infiltration. Darvan C-N, manufactured from Vanderbilt Minerals, is an ammonium polymethacrylate dispersing agent for ceramic bodies. Graphene powder, under

catalog of xGnP-M-5 manufactured from XG Sciences, was used to help reduce cracking in the ceramic pastes. Both pastes were created from their components using the following method:

1. The compositions listed in Table 1 were mixed using a Resodyn Acoustic Mixer LABRAM at an Intensity value of 0.9 for 5 minutes.
2. Air bubbles were then removed from the mixture using the ultrasonic cleaner for 15 min.
3. The paste is then placed into the vacuum pump. The vacuum pump has the pressure released on it approximately every 20 seconds or whenever the paste started to visably rise. Vacuum pump was used until no more air bubbles appeared in the solution, approximately 5 minutes. Pastes were stored at room temperature in a closed container.

3.3.2 Calcium Sulfate Mold

Calcium Sulfate, manufactured from Plaster of Paris, was also explored as a ceramic mold material for this project. To create the paste, two parts $CaSO_4$ were mixed with one-part water by volume ratio. Paste was placed in vacuum pump for approximately one minute. This paste does not undergo the same procedure to remove air bubbles because it solidifies very quickly without heat (while $CaCO_3$ paste needs heat and solidifies at a much slower rate when left in air). This mold material needs no additional ingredients and forms a strong structure, but it is difficult to remove. The paste then undergoes the infiltration process presented in the next section.

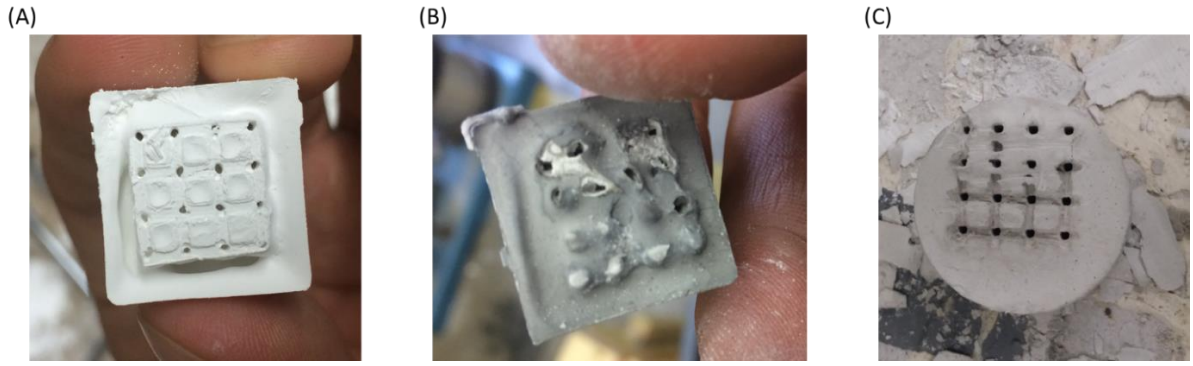

Figure 12: The three different types of paste after they have been sintered all using the unit cube scaffold for their design. (A) Guar Gum binder based paste. Exhibits a white color, similar to $CaCO_3$. (B) Sodium Silicate binder based paste. Exhibits a gray color from the addition of graphene that has not been burned off. (C) $CaSO_4$ paste

3.4 Infiltration of PLA Scaffold with Ceramic Paste

In Figure 12, a ceramic shell can be seen around each of the scaffolds to provide support to the structure during burn off. To produce this ceramic shell and perform the infiltration of the paste, two custom-made, 3D printed parts were created. These parts, a printed 'cup' and 'hollow cylinder' can be seen in Figure 13 and were designed to create a shell with the diameter to fit into the steel pipe apparatus described in section 3.6. The process begins by placing the PLA printed scaffold into the circular printed cup. This apparatus holds the paste while it solidifies and creates a cylinder of support for the infiltrated ceramic mold. It is also easily removed by the burnout process presented in Section 3.5. The second apparatus is a hollow cylinder the fits the PLA cup snuggly. This hollow cylinder is twice the height of the designed PLA cup and is strong enough to be placed into the Resodyn acoustic mixer and withstand its gripping and vibrations. This cylinder allows for paste to be added to the cylinder without creating a mess and allowing excess paste to be added to completely fill the scaffold and cup.

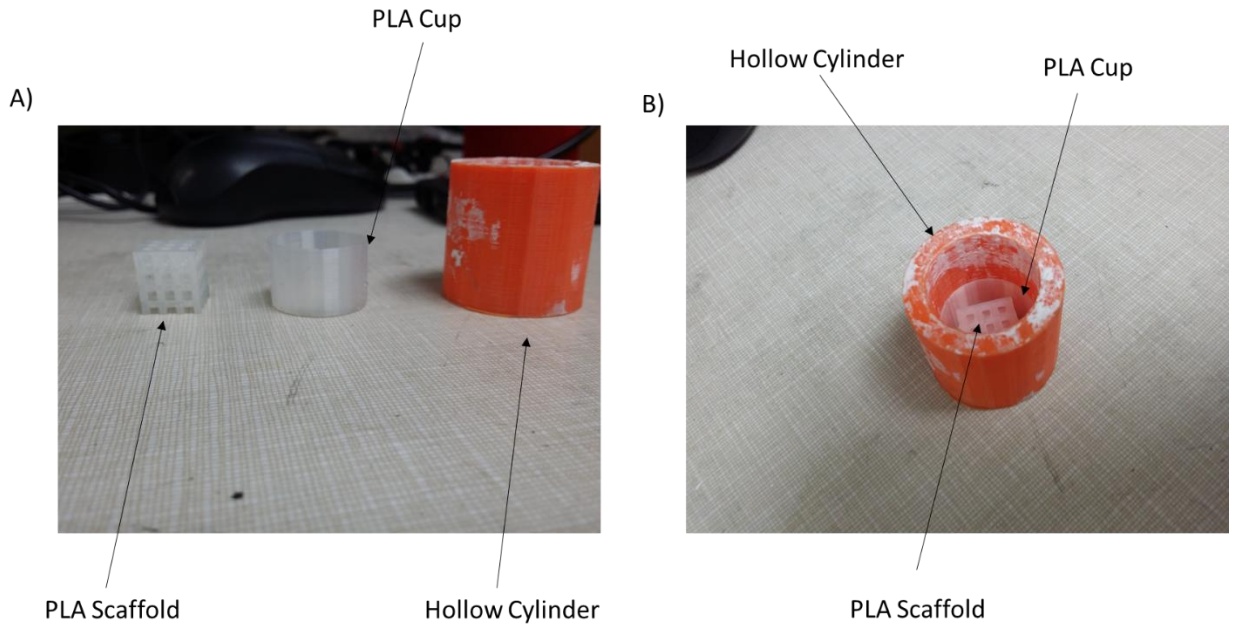

Figure 13: Photo of Infiltration Apparatus. (A) The scaffold, PLA cup, and hollow cylinder used for infiltration. (B) The assembled apparatus to be put into the acoustic mixer.

The $CaCO_3$ paste is too viscous to directly pour into the constructed apparatus but can be added with the help of a scoop or wooden tongue depressor. The $CaSO_4$ paste is much more viscous and will flow easier if much time has not elapsed since it was originally mixed. For this reason, it is recommended to add a shell of tin foil to the hollow cylinder to prevent leakage of $CaSO_4$ paste. The hollow cylinder apparatus is then placed into the acoustic mixer and run for two minutes at 20% intensity. The vibrations allow the paste to infiltrate the pores of the PLA Scaffold. The PLA cup with the PLA scaffold are then removed from the hollow cylinder, which can be cleaned and reused to infiltrate the next sample.

3.5 Removal of PLA Scaffold and Sintering of Ceramic Mold Materials

Removal of PLA scaffold was performed by a burnout method. The samples (cup, scaffold, and paste) were placed into a furnace and heated by the following ramp cycles:

Table 4: Ramp cycles for the heating of the three ceramic pastes

Steps	$CaCO_3$ Paste 1	$CaCO_3$ Paste 2	$CaSO_4$ Paste
Overnight Drying	-	-	Left Overnight
Ramp 1	1°C/min to 100°C	1°C/min to 100°C	1°C/min to 100°C
Hold Time	60min	60min	60min
Ramp2	5°C/min to 400°C	5°C/min to 400°C	5°C/min to 400°C
Hold Time 2	60 min	60 min	60 min
Ramp 3	5°C/min to 1000°C	5°C/min to 700°C	5°C/min to 700°C
Hold Time 3	60 min	60 min	60 min

These ramp cycles were determined from trial and error trying to determine the factors to reduce cracking, perform an optimal PLA burnout, and optimize the calcification of the calcium carbonate ceramic. The first ramp cycle to 100°C is used to slowly remove any excess water in the samples at a slow rate to reduce cracking. The thermal degradation of PLA occurs at approximately 400°C and produces different compounds such as low molecular weight molecules and linear and cyclic oligomers with different molecular weight and lactide[54]. Fumes were vented using an overhead fume hood. The pastes are brought to 700°C to sinter the bonds of the $CaCO_3$ ceramic and to help remove any remaining PLA left from the burnout. Paste one is sintered at 1000°C to strengthen the ceramic bond and convert the $CaCO_3$ to Calcium Oxide (CaO) by the following equation:

$$CaCO_3 \rightarrow CaO + CO_2$$

Equation 3: Decomposition reaction of Calcium Carbonate to Calcium Oxide and Carbone Dioxide (CO_2). This reaction occurs at approximately 800°C.

The sintering of the $CaSO_4$ mold to 700°C is necessary to remove a film of PLA that forms on the pores of this mold material. Blocks of graphite were placed next to the $CaCO_3$ paste apparatus's

in the oven in order to flood the chamber with carbon and help avoid the decomposition reaction observed in Equation 3. All samples are left in the oven overnight to cool naturally back to room temperature.

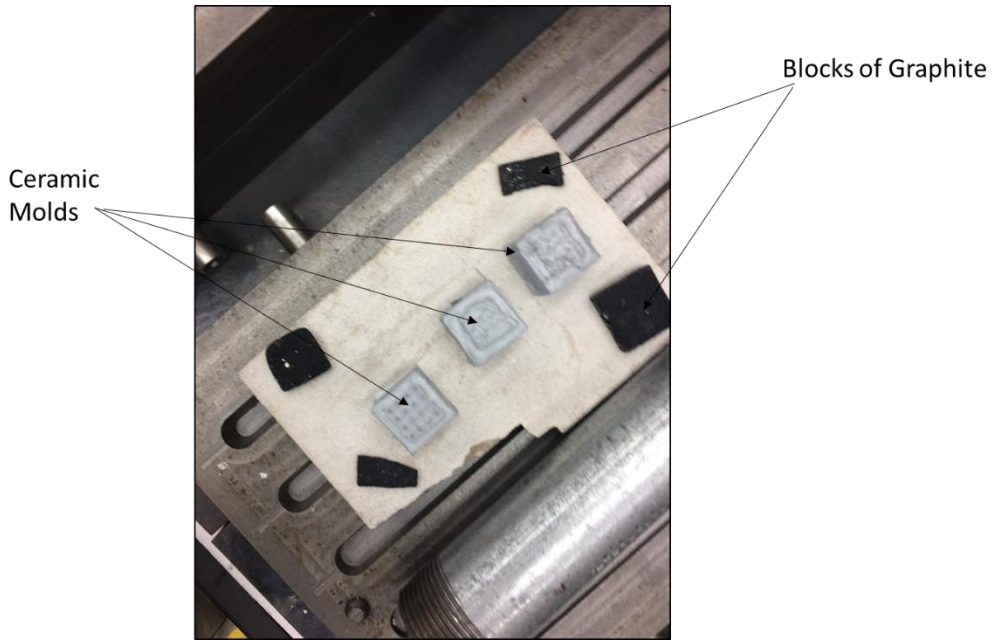

Figure 14: Setup for the removal of the PLA from the ceramic mold.

3.6 Infiltration of Ceramic Mold with Metal

A 1“ black steel pipe and cap are used to perform the infiltration of the ceramic molds with the desired metal. The overall apparatus can be seen schematically in Figure 15. A pipe cap is filled near the top with kaowool so only a few top threads of the cap are exposed. The ceramic mold scaffold is then placed on top of the kaowool, the black steel pipe is attached to the cap, and a cylinder of metal is placed on top of the ceramic mold inside the steel pipe. The pipe is open to the atmosphere. Both the pipe and cap are coated with graphite spray to prevent the metal from sticking to the walls of the pipe and from infiltrating into the pipe’s threads. This allows for easier removal of the scaffold from the pipe after infiltration.

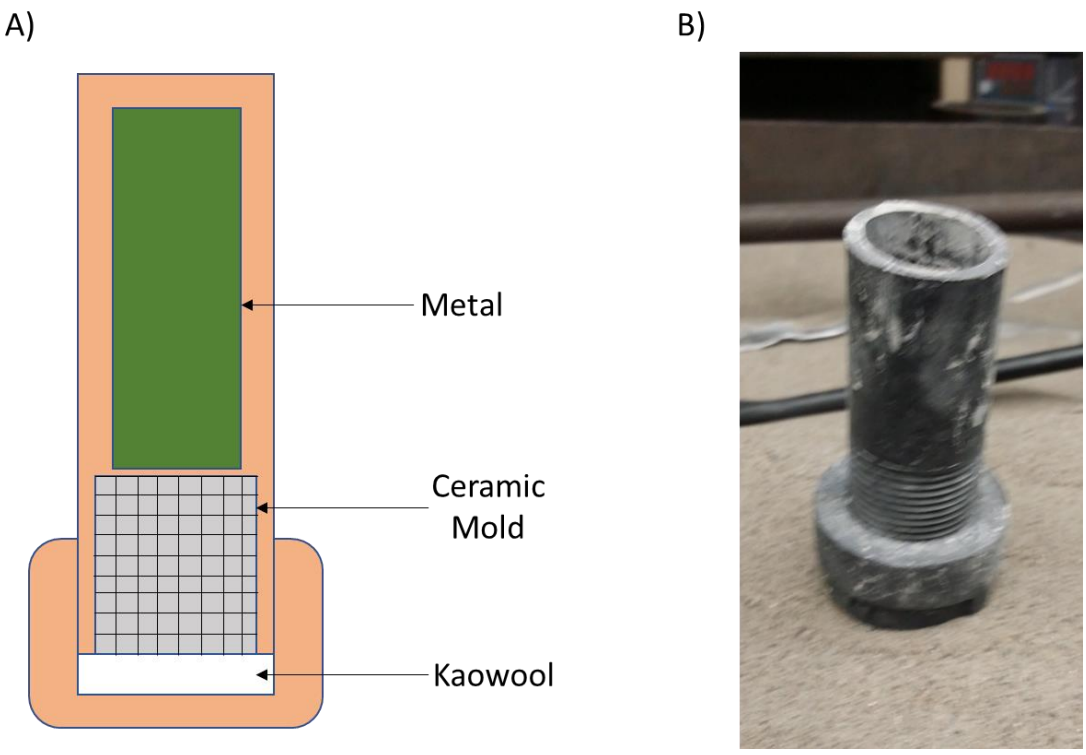

Figure 15: Schematic of pipe apparatus used for metal infiltration of ceramic mold. (A) Drawn schematic of inside of black pipe. (B) Photo of outside of pipe setup.

The assembled pipe apparatus is then placed into a pressure infiltration furnace that is sealed and evacuated of air until the pressure of the vessel reads a negative value. The furnace is then ramped to 680°C for magnesium and 540°C for Zinc and held for 30 minutes. After the allotted time, the vacuum valve is closed, vacuum turned off, and ultra-high purity argon gas was released into the furnace to perform the infiltration of the metal into the ceramic mold. Pressure used for infiltration varied depending on the pore size of the ceramic mold but, in general, a pressure of 140 pound per square inch (PSI) was used to perform infiltration. Thirty minutes after pressure of vessel is increased the furnace is turned off and allowed to cool.

Samples can then be pressed out of the steel tubes, often needing a hammer and chisel. The steel pipe and cap are then clean and recoated with graphite spray to be used in future trials.

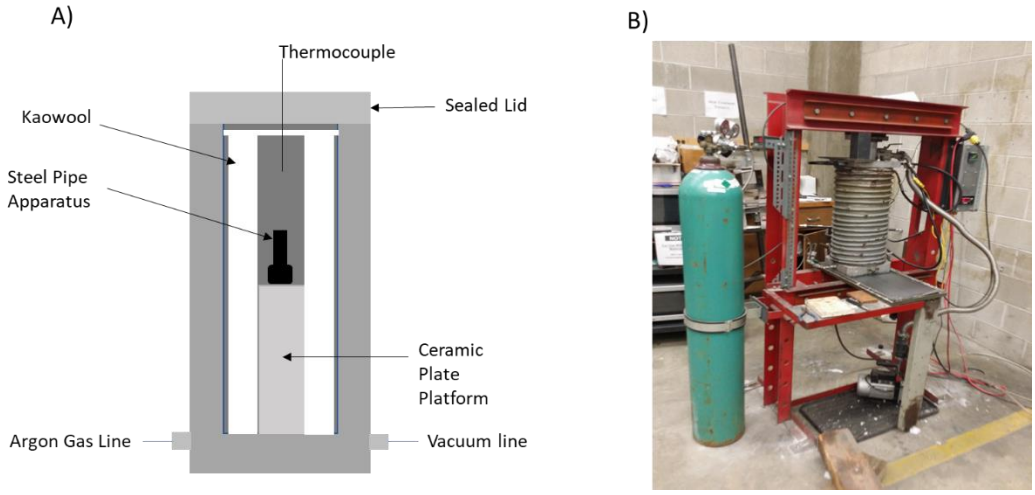

Figure 16: Schematic of pressure infiltration process. (A) Cross section showing inside of furnace. (B) Image of pressure infiltration furnace with vacuum and argon gas canister visible.

3.7 Dissolving of Ceramic Mold Material

Excess metal, like that seen in Figure 3, is removed from the metal infiltrated mold by using a hacksaw. Each of the three types of ceramic molds have a different process for their dissolution from the metal scaffolds. Ceramic mold 1 is the easiest to removed, as it is brittle by nature. The mechanical vibrations from the removal of the mold from the steel pipe are strong enough separate the mold from the metal scaffold. Any remaining ceramic can be removed by placing the scaffold into a steel cup filled with ethanol and then placed into the acoustic mixer at an intensity of 10% for up to three hours. Ceramic mold 1 was brought to a higher temperature than the other molds to convert the calcium carbonate to calcium oxide. The calcium oxide has a reaction with ethanol by the following reaction:

$$CaO + 2C_2H_5OH \rightarrow Ca(OC_2H_5)_2 + H_2O$$

Equation 4: Calcium Oxide reaction with Ethanol used for the dissolving of ceramic paste one.

The combination of mechanical vibrations and the reaction in Equation 4 are enough to separate the remaining mold material from the metal scaffold. Water was also found to be effective at dissolving calcium oxide and can be used with zinc samples but was avoided when used with magnesium because of the reaction displayed in Equation 1.

Paste 2, the $CaCO_3$ paste that uses sodium silicate as a binder, proves to be more difficult to remove. The addition of the sodium silicate binder causes a significant increase in strength of the ceramic material. The same methods that were used for paste 1 were attempted on paste 2 but to no avail. Different solutions were tested for the dissolution of mold material but with no positive results. Strong acids were able to remove the calcium carbonate paste but had a strong corrosion effect on zinc and magnesium. Hydrofluoric Acid, due to its dangerous nature, was not tested with this sample but has been used in literature to remove mold material from magnesium scaffolds without sacrificing the integrity of the metal. However, this experiment looks at providing a safe method for producing magnesium scaffolds and because of that dangerous, bone burning chemicals were avoided. Mechanical methods were found to be partially successful. A drill with a small enough drill bit was able to remove the mold material but that will prove troublesome as the pore structure of the scaffolds get more complicated.

Paste 3, the $CaSO_4$ paste, was found to be dissolved in a weak base, sodium bicarbonate. The reaction between sodium bicarbonate and calcium sulfate produces sodium sulfate and calcium carbonate as seen in Equation 5:

$$Na_2CO_3 + CaSO_4 \rightarrow Na_2SO_4 + CaCO_3$$

Equation 5: Reaction of Calcium Sulfate with Sodium Bicarbonate

This reaction has a negative Gibbs free energy of reaction (-29.5 kJ at standard temperature and pressure) meaning the reaction will proceed spontaneously. However, the reaction still proceeds slowly, so heat is added to help speed up the kinetics of the reaction. The sample is placed into warm water (approximately 68°C) with a stir rod. Sodium bicarbonate is added until the water turns a cloudy white color and the mixture is left stirring for approximately one hour. The beaker holding the solution and sample is then removed from the stirpad and placed into the ultrasonic cleaner for 45 minutes. The dissolution of paste occurs best if the solution is placed into the ultrasonic cleaner while still in warm water with sodium bicarbonate. The solution is then removed, and the process is repeated approximately five times to remove all of the mold material.

Figure 17: Apparatus of dissolving calcium sulfate from metal scaffold. Picture is a stir plate with the scaffold apparatus inside, baking soda, and water.

3.8 Mechanical Testing and Microscopy

The samples were compressed using an Instron 250kN universal testing system. To ensure alignment between the top and bottom platen against the specimen for the duration of the test, a compression fixture was used and can be seen in Figure 18. Scaffolds were compressed at a rate of 0.250 mm/min.

Figure 18: Scaffold in compression testing fixture

Compression data was analyzed for the following mechanical properties: stiffness, compressive strength, densification point, and toughness. Compliance from the compression fixture was subtracted from the compression data and then the mechanical properties were found using a custom R script for data analysis.

The hardness and fracture toughness were tested by nanoindentation machine. Indentation was performed on struts of samples that were mounted and polished. The Vickers hardness (HV) and facture toughness (K_{IC}) were calculated from the following equations:

$$HV = \frac{0.1891 * F}{d^2}$$

$$K_{IC} = 0.0824 * \frac{F}{C^{\frac{3}{2}}}$$

Equation 6: Calculations for Vickers hardness and fracture toughness

For microscopy analysis, samples were cut and mounted into thermoplastic molds. These samples then were ground and polished using 320, 400, 800, and 1200 grit SiC paper from Buehler. The magnesium samples were then polished using 1 micrometer diamond slurry while the zinc samples were polished using silica. The etchant used for magnesium was 150 mL ethanol, 50 mL deionized water and 1 mL glacial acetic acid. The samples were held submerged in the etchant solution for 14-120 seconds with slight agitation, rinsed with ethanol, and dried using an air gun. The etchant used for zinc samples was 100 mL ethanol and 3 mL hydrochloric acid. These samples were submerged for 50 seconds, rinsed with ethanol, and dried using an air gun. Macroscopic structure of foams was examined with a Zeiss Stemi2000-C stereomicroscope, and the microstructure was observed using scanning electron microscopy (SEM). Energy-dispersive X-ray spectroscopy (EDS) and X-ray power diffraction (XRD) were used to determine compositions of the scaffolds after reactions with the mold materials. TGA was ran to determine the burn off temperature of specific binders. TGA was ran with an ramp of 10°C/min with an isothermal hold of 5 minutes.

3.9 Determine of Pore Size and Porosity

To determine average pore size and porosity of the tissue engineering scaffolds, they were first imaged using the Zeiss Stemi2000-C Stereomicroscope using the Axiovision software. After imaging, the length of randomly selected pores and beams were selected and measured using the length function in Axiovision. This is an initial estimation to get a ballpark estimation of where the pore size is. After measuring the pore size in AxioVision, the images were placed into ImageJ software for further analysis to measure the size of all pores and to determine the porosity of the structure. The following procedure in ImageJ was used:

1. Open ImageJ and load the desired picture for analysis
2. Set scale by selecting the line tool and drawing a line on the scale bar of your image. Then select Analyze > Set Scale. The Set Scale window will pop up and the user needs to input the scale and its appropriate units into the 'known distance' box and the 'Unit of length' box. For tissue scaffolds, this will mostly be done in microns.
3. Optional step to crop the image for cleanup or to remove unnecessary portions of it.
4. Greyscale and threshold image to isolate the pores. To greyscale follow the path: Image > Type > 8-bit. Then, Image > Adjust > Threshold to threshold the image. The automatic threshold calculator usually does an excellent job of isolating the pores, but the slide bars can be moved to alter the threshold to the desired. Once threshold is to the desired level, click apply and close the window.
5. Optional: Clean up of image to remove noise. Process > Noise > Despeckle and Process > Noise > Remove Outliers.

6. Select the measurement parameters that the ImageJ software will calculate. The 'Set Measurements' option can be found under the Analyze dropdown menu.
7. Analyze the pore size by selecting 'Analyze Particles' under the Analyze dropdown menu. This brings up a popup window with a plethora of options. The first trial should be run with size > 0-Inf and circularity > 0-1. Display results and summarize should have their boxes checked and the show box can be selected to the user's preference. Press OK to continue.
8. The results box will show each pore picked out by the algorithm along with all their calculated values. The summary box will summarize this data.
9. In the results section, the area of the pores can be looked at to see the values that represent noise (they are significantly smaller when compared with other pore values). Step 7 can be repeated with a change in the size function to remove the noise and to isolate the pores.
10. The important info in the summary box is the '%Area' box which gives the images porosity. For the calculated pore size of the unit square scaffolds, the items 'Width' and 'Height' are averaged to calculate the pore size. For circular pores, the Ferets height can be used. Then all pore sizes in the image are averaged to give the average pore size for the structure.

Individual pore sizes can be measured in ImageJ using the measure function, however, the above listed function will measure all the pores at once, giving a more quick, accurate result. In the case of not square pores, the boneJ plugin can be used to easily calculate average pore size and average distance between pores[55]. Simply follow the same procedure to threshold the

image and then click plugin > boneJ > thickness. Check the desired boxes for the information desired and the results box will show 'Tb.Th mean' which is the average pore size. This method is quicker and requires less user input but the algorithm is optimized to measure circular pores and underestimates the size of square pores. Note that bonej's calculation for average distance between pores (beam size) is computationally intensive and may take a few minutes to run to completion.

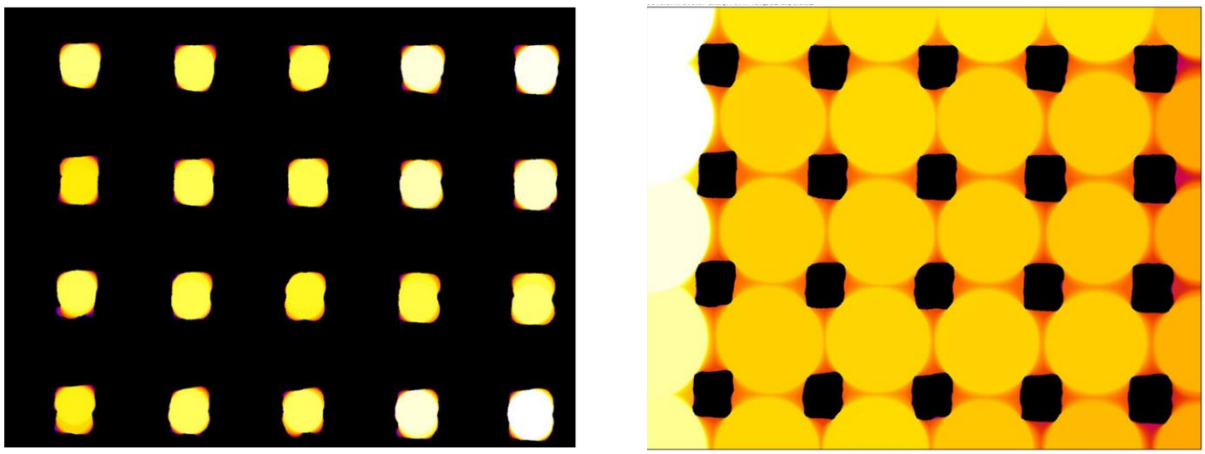

Results

File Edit Font Results

	Label	Tb.Th Mean (unit)	Tb.Th Std Dev (unit)	Tb.Th Max (unit)	Tb.Sp Mean (unit)	Tb.Sp Std Dev (unit)	Tb.Sp Max (unit)
1	pla_800um_red.jpg	630.444	121.230	757.595	1757.442	254.233	2340.465

Figure 19: Example results from BoneJ analysis. Pore map (in black) used to calculated pore size, distance map (in yellow) used to calculate distance between pores, and results table.

To calculate distance between pores (strut size) the ND package in ImageJ was used[56]. ND stands for nearest distance and the package was developed to calculate the average size and distance between pores and their nearest neighbors in a porous scaffold. The programs algorithm calculates the centroid of each pore then uses a distance between two points formula to calculate the distance. The 'thickness' is the output value we are interested in and it is calculated by subtracting the radius of both pores from the distance value. It is worth noting

that for large pored scaffolds, pore and beam size can be quickly and manually measured with the measure function and drawing lines.

CHAPTER FOUR: RESULTS AND DISCUSSION

This project began with the vision of 3D printing a calcium carbonate paste using a direct ink writing method of 3D printing. The calcium carbonate would serve as a spacer material for metal foam infiltration. However, this method proved to have numerous problems. First, the paste had to have a finely tuned viscosity to be able to print and hold its printed form. Another problem was that the paste took too long to solidify without an external heat source to dry it layer by layer. The build plate of the 3D printer was heated and allowed for the first few layers to dry quickly; however, when the printhead was too high above the heat source the calcium carbonate mold material would not dry. This led to poor layer adhesion and the collapse of the mold as undried material did not have the mechanical strength to hold its form. Lastly, since the paste lacked the ability to quickly dry, it also lacked the ability to create bridge structures needed to create pores in a three-dimensional scaffold. A sacrificial support structure would be needed to create a 3D scaffold-mold from the calcium carbonate paste. PLA was considered for dual head extrusion, but there was poor layer adhesion between the paste and the thermoplastic, leading to the collapse of the structure.

The idea of using a thermoplastic support structure led to the process presented in this thesis. Instead of using a dual head extrusion to create a support structure, it was decided to print the support structure and then infiltrate it using the paste. From there, the support structure could be removed, leaving the mold material for infiltration. This results section is a culmination of the designed process covering the design of the mold material, its interactions with magnesium and zinc, microscopy of the final scaffolds, and the mechanical properties of those produced scaffolds.

4.1 Design of Calcium Carbonate Mold Material

Calcium Carbonate was chosen as the ceramic mold material because of calcium's positioning in the Ellingham Diagram (Figure 20). Calcium is one of the few elements that reacts to form oxides quicker

than magnesium and can serve as a reducing agent for magnesium. Additionally, calcium carbonate has the ability to form a solidified ceramic structure as proven by previous experiments performed in our lab.

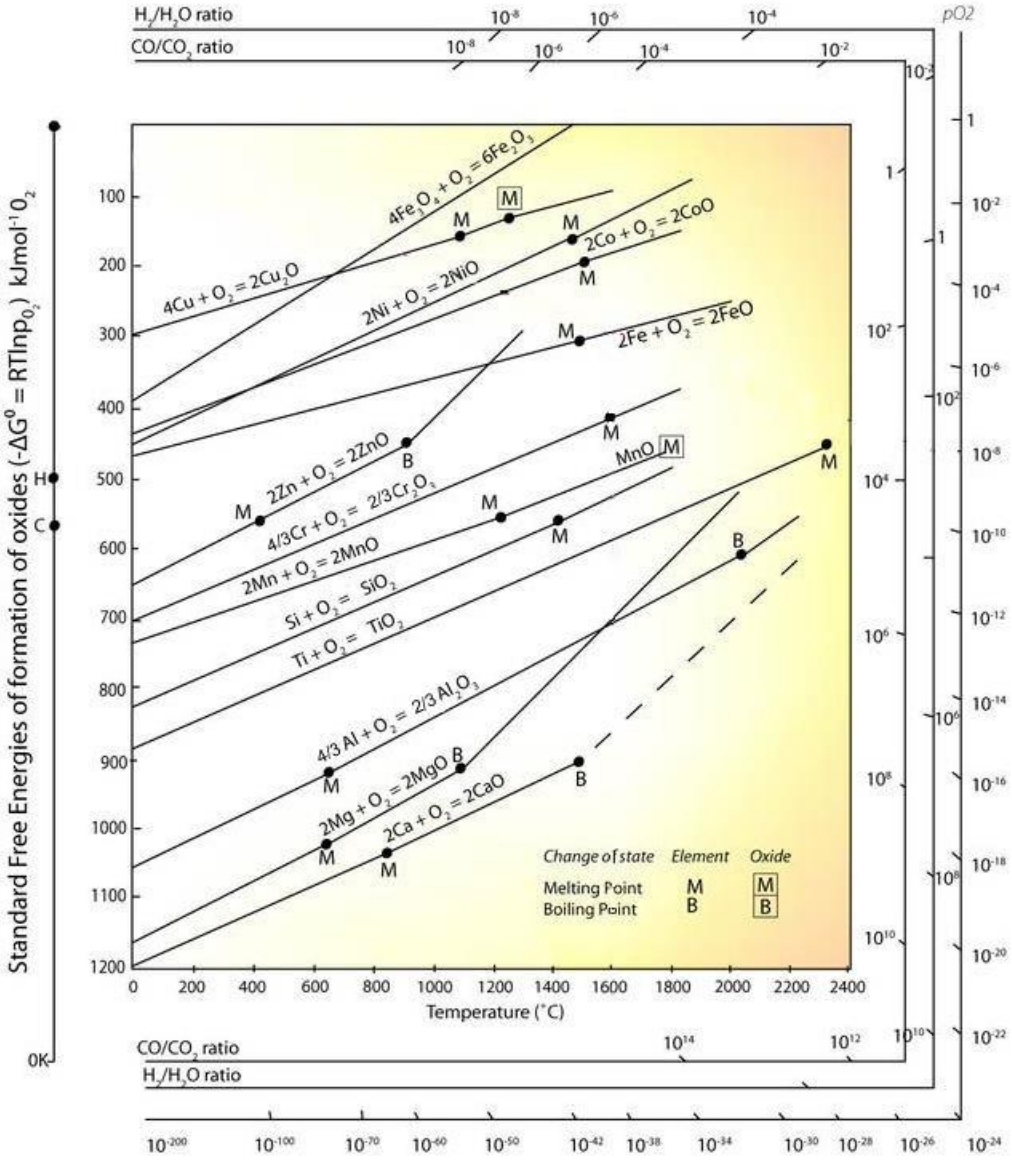

Figure 20: Ellingham diagram for oxides.

With a ceramic material chosen, the next step was to determine how to best make it a paste that could be 3D printed. While the 3D printed method was eventually abandoned, this paste composition was determined to still be optimal to fulfill the infiltration process described in Section 3.6. The first factor

that had to be determined was how water addition to calcium carbonate powder effected the consistency of the ceramic. Obviously, more water would make a less viscous paste, but the experiment presented in Table 5 shows that one mL aliquots of water were added to a set amount of calcium carbonate to determine its consistency at each step.

Table 5: Hydration of calcium carbonate and guar gum binder addition. Starting at step six, each step is given one minute in the acoustic mixer

Steps	CaCO3(g)	Water(ml)	Guar Gum(g)	Comments
1	25.8			Only CaCO3 Powder
2		1		
3		1		
4		1		
5		1		
6		1		
7		1		First indication of paste forming
8		1		Creates a ball when shaken in mixer
9		1		
10		1		Makes finger like pattern up cup when shaken (Figure 21)
11		1		
12		1		Finally fluid enough to flow when tilted.
13			0.5	Thickens quick
14			0.5	Thickened too quick
15			0.5	Balled up; easy cracking, crumbles
16		2		No change

Once a desired consistency was chosen, the green strength of the paste had to be increased while still maintaining the fluid consistency of the paste. Two binders were chosen to test for this step:

methylcellulose and guar gum. Similar hydration experiments, as in the previous step, were used to determine how the binders effected the consistency of the calcium carbonate paste and one methylcellulose trial can be seen in Table 6.


Figure 21:Paste consistency and spider like mixing.

Table 6: Step by Step Addition of Methylcellulose to calcium carbonate paste

Step	CaCo3	Water Added	Methylcellulose Added	Comments
1	50.0052			
2		18		
3			0.099	Liquid consistency
4	50.036			
5		4		
6		2		
7		2		
8			0.194	
9		2		
10			0.058	
11			0.066	
12			0.056	
13			0.054	
14			0.065	Great paste consistency

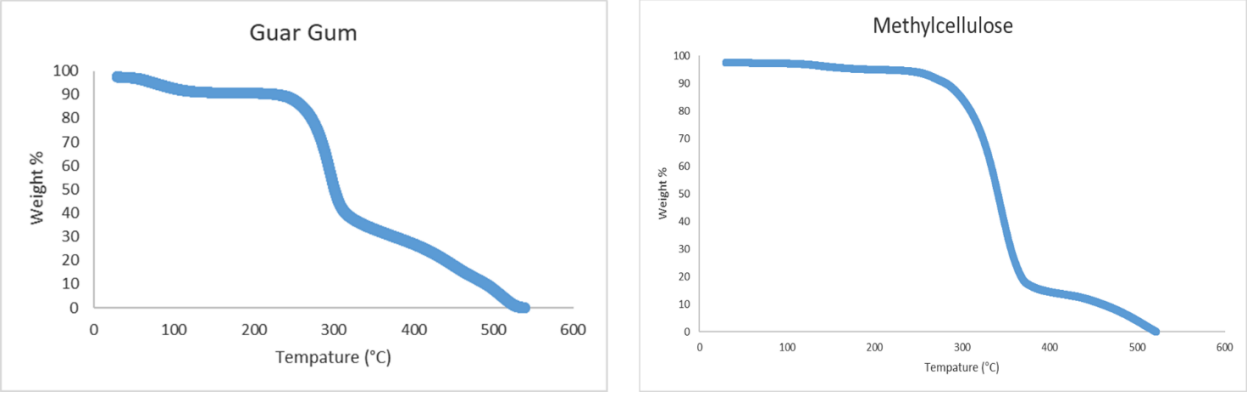

Figure 22: TGA analysis of binder types for ceramic paste.

Generally, less guar gum was needed than methyl cellulose to achieve the same kind of thickness and consistency in the paste. With paste consistencies chosen, it then had to be determined how well these binders held together throughout the remaining steps of the process. Both pastes containing their respective binders were put through the infiltration and burnout steps (Sections 3.4 and 3.5) but these harden molds were found to mostly lack strength and would often crumble at slight disturbances. Thermogravimetric analysis (TGA) was performed on binders to determine the temperature the binders would burn out of the mold material (Figure 22). From the TGA, guar gum was determined to have a higher weight percentage left at 400°C than methylcellulose. Because of this, it is believed to create a more stable mold material and was used for a binder instead of methylcellulose.

Choosing the best method for the removal of the PLA scaffolds from the mold material was another problem that the project encountered early on. Bringing the samples to high temperature was the easiest way to separate the PLA from the mold material. However, in the beginning, these samples would fall apart and crumble or have major cracks in them. This was caused for a number of reasons. The major reason was because the samples underwent heating without a controlled ramp. The extreme change of temperatures caused heat shock, leading to cracking of the samples. The samples also lacked structural support as a ceramic shell was not yet added for support. Additionally, the samples

underwent PLA removal in one furnace and were then moved to a different furnace for final sintering. This was because the first furnace could not reach >800°C and the second furnace was not near a vent to remove the fumes of the plastic burn off. This shuffling of samples and quick temperature changes from one furnace to open air and back to another furnace could also have caused cracking from heat shock.

To attempt to remedy this problem, the dissolution of the thermoplastic after infiltration was attempted. Two types of thermoplastic scaffolds were created for this trial: ABS and PLA. ABS can be dissolved in acetone and PLA can be dissolved in chloroform. Neither of these two chemicals influenced the calcium carbonate mold. These dissolution trials showed merit as completely evacuated mold materials with no cracking were recovered. However, the dissolution of the thermoplastics would also cause the breakup of the calcium carbonate material into chunks, in some trials, as can be seen in Figure 23.

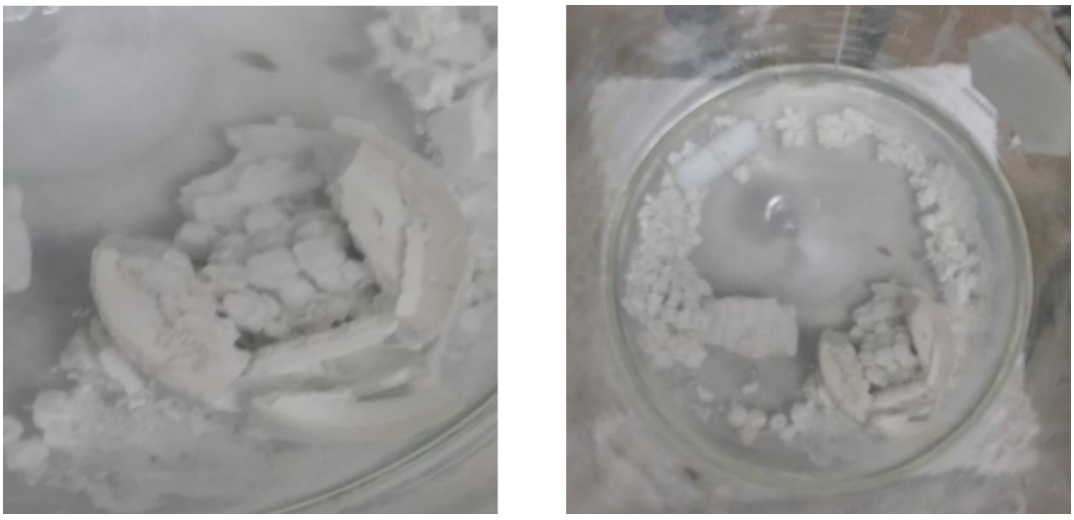

Figure 23: Image of mold material falling apart in chloroform solvent.

It is important to note that the calcium carbonate paste never dissolved in these dissolution studies, only the thermoplastic. The calcium carbonate mold seems to break into chunks in the failed trials, possibly a side effect of the stress of the inside structure dissolving. Many trials created mold materials

that did not break apart but there was no clear reason for the inconsistency of these results. Because of these inconsistencies, the dissolution route was abandoned for the removal of the thermoplastic scaffold in favor of the burn off method with a ramp.

4.2 Reaction of Mold Material with Magnesium

The production of magnesium foams has been troublesome with the designed method. The exact reason is unknown as previous work with the calcium carbonate mold material and magnesium has had different results then what is presented in this thesis. Figure 24 shows the results from one of the trials

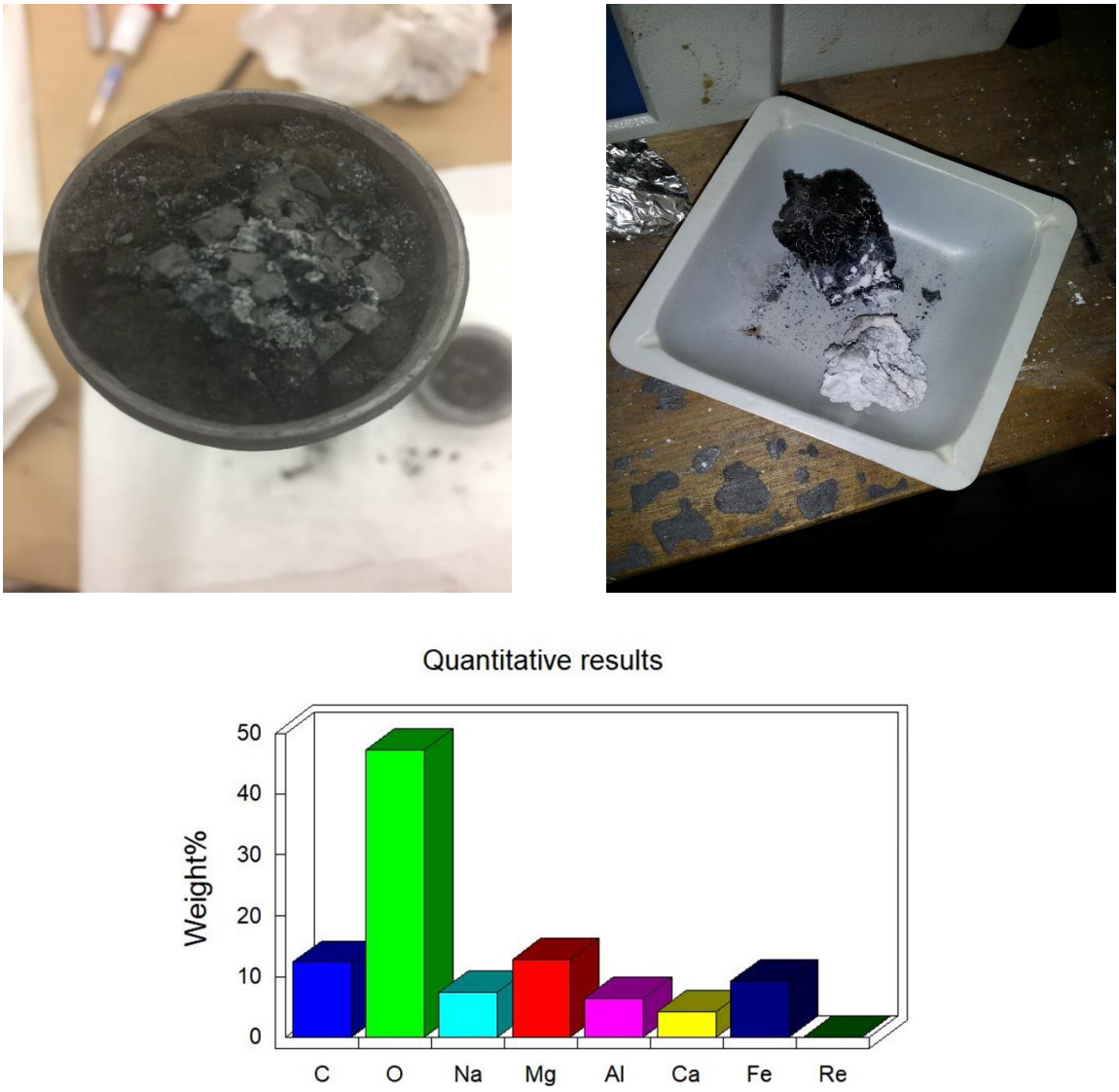

Figure 24: Reaction of Magnesium with mold material and EDS analysis.

using paste two and AZ91D, the most widely used magnesium die cast alloy that is mostly magnesium and aluminum with trace amounts of copper, iron, nickel, zinc, and manganese. In this figure, we can see blackened magnesium and whitened magnesium, signs of oxidation. Similar results were seen in trials with the other pastes. In some experiments, infiltration of the mold material occurred, but the same blackened magnesium result was present. EDS analysis of the magnesium after infiltration shows high amounts of oxidation occurring. Additionally, there are relatively high levels of both carbon and iron present in the sample. This could be indicative of a reaction occurring between the steel pipe and the magnesium or the graphene spray and the magnesium. The high temperature and pressure of the infiltration process could be fueling reactions between magnesium and the other objects in the infiltration apparatus as previous experiments with this setup were not done under high pressure. The most obvious source of oxidation would be from a reaction between the mold material and the

Figure 25: Magnesium oxidation without mold material and EDS of the reaction.

magnesium, but this same blackened magnesium occurs when only magnesium is melted in the steel pipe cap. This could mean that there is a reaction between the magnesium and the furnace, leading to the oxidation or perhaps not a perfect seal allowing oxygen to enter the atmosphere.

To test if this oxidation occurs without the presence of the mold material or high pressure, an experiment was run in the absence of both. In this experiment, a cylindrical slice of AZ91D was placed upwards on a steel pipe cap and placed into the pressure infiltration furnace. The furnace was sealed and the vacuum was turned on until the pressure sensor read a negative value, indicative of a fully evacuated system. The furnace was then raised to 540°C. An interesting thing occurred during this experiment. A fuse blew and the furnace only reached a temperature of 460°C and was allowed to cool to room temperature. The removed sample was taken out and found to have oxidized on the top even though the sample had not melted (Figure 25). This is significant as it shows that the sample is reacting with the furnace without the addition of any other materials and before melting temperature even occurs. The EDS analysis shows high amounts of oxidation occurring although not as high as in the previous analysis. The exact cause of this oxidation is still uncertain but there is a clear connection between the furnace and the oxidation of the magnesium sample, meaning it is not believed that the mold material is causing the oxidation of the magnesium sample and that this could be a promising route still for the casting of magnesium foams. Since magnesium was not able to be produced, it was decided to cast the scaffolds out of zinc, which is a biocompatible metal that has been emerging the last few years as a possible biomaterial for tissue engineering scaffolds.

4.3 Creating Zinc Unit Squares of Three Variable Pore Size

Three models were designed in Creo Parametric to be cast in zinc through the methods described in Chapter Three. The models were chosen to be made up of a square unit cell of decreasing size to create three models that have varying pore and strut size. Pore size refers to the length of empty space between two solid struts in the model. In the case of these three models, the pore size refers to the length of the pore straight across. Strut size refers to the length of solid between two pores. The pore size of the three models are 2.50, 1.75, and 1.00 mm with respective strut sizes of 1.50, 1.25, and 1.00 mm. All three models were designed with a length and width of 15 mm and a height of 17 mm. The intention of this experiment is to determine how closely the metal cast parts related to the original CAD design and similarly how the 3d printed PLA parts relate to their original CAD design. A higher strut size was chosen than is typically expected of a tissue engineering scaffold (leading to a lower porosity) to make sure infiltration occurs. It was not known what the limiting mold pore size was where infiltration

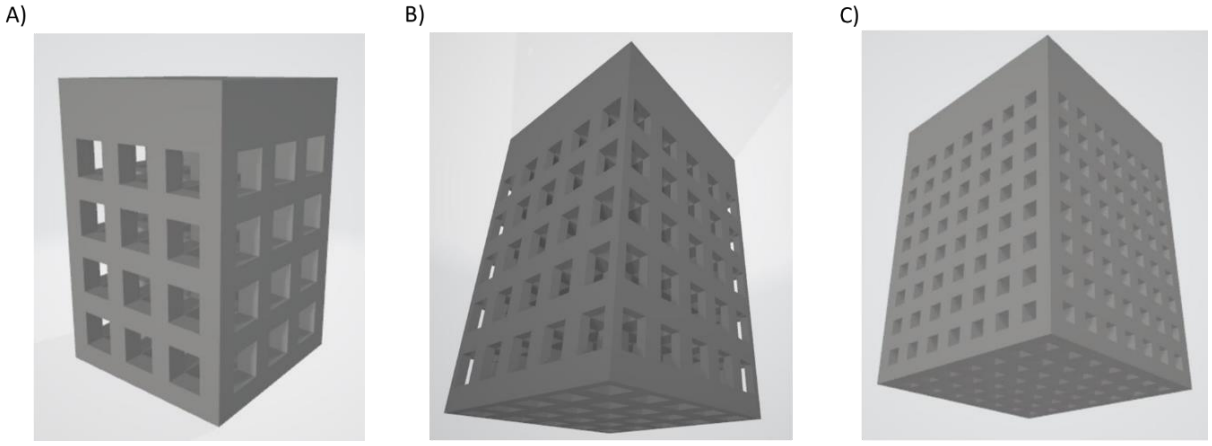

Figure 26: CAD models of the three scaffolds of variable pore size to be replicated in metal.

would no longer occur, but scaffolds with porosity > 60% have been produced in later experiments following this method. It is the goal of this section to identify the physical changes in pore size that occurs from the original CAD design to the PLA prototype models to the final metal models through microscopy. Then, SEM images will be analyzed to look at the metal structure on a microlevel, observing

any micro porosity that occurs, and lastly, the mechanical properties between these three models will be compared.

4.3.1 Deviations from CAD model to PLA model

When 3D printing normal sized structures, the dimensional accuracy of the prints is accurate with low error. However, this small error has a larger effect when creating small porous structures as each pore is subject to this error. This effect can be seen in Figure 27, where the center pores are visually smaller than the outside pores in the first image. The original CAD design has all pore sizes being of the same size, but the printing process causes a variation of pore size to occur. This variation in pore size is what is being examined, as well as how it differs from the original CAD design and the final metal structure.

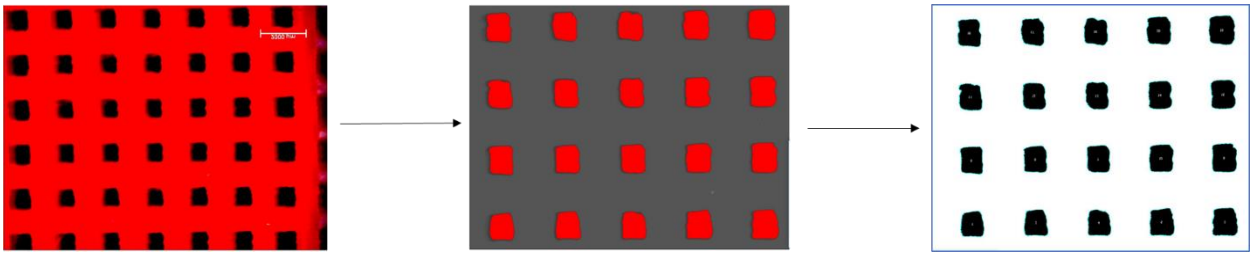

Figure 27: Small pore sample ImageJ analysis process from image to pore size map

When the CAD model is printed, the PLA models were found to have an increase in beam thickness and a decrease in pore size (Table 7, Figure 28). Additionally, these results are compared with the CAD designs and their zinc counterparts in Figure 30. These deviations from the CAD model could be a result of many factors including faults in the printer settings, slightly unleveled print bed, to big of a print head for this size of dimensional accuracy, expansion of the thermoplastic that occurs during its cooling, or simply the result of the dimensional accuracy of the printer. An 18% percent decrease in pore size was found in the small scaffold, a 10% decrease in the medium scaffold, and a 9% decrease in pore size for the large scaffold from the original CAD design. This could point to a limitation in the printer when designing structures of small size that could be remedied with a smaller print nozzle or an investment into a printer that has been designed for printing small parts. Both printers used in this project are not

designed for the printing of this small of parts. There are many printers on the market that are designed for small dimensional accuracy but would require a higher capital investment. We will examine the pore size distrubution in the final models later on and determine if the project would benefit from a better quality printer.

Table 7: Summary of pore size data for 3d printed PLA scaffolds

	Mean Pore Size (µm)	Mean Beam Size (µm)	Percent Change in Pore Size	Percent Change in Beam Size	Porosity (%)
PLA Small Scaffold	817.19	1111.90	-18.28%	11.19%	16.3
PLA Medium Scaffold	1571.47	1342.45	-10.20%	7.40%	30.89
PLA Large Scaffold	2276.77	1724.96	-8.93%	15.00%	33.03

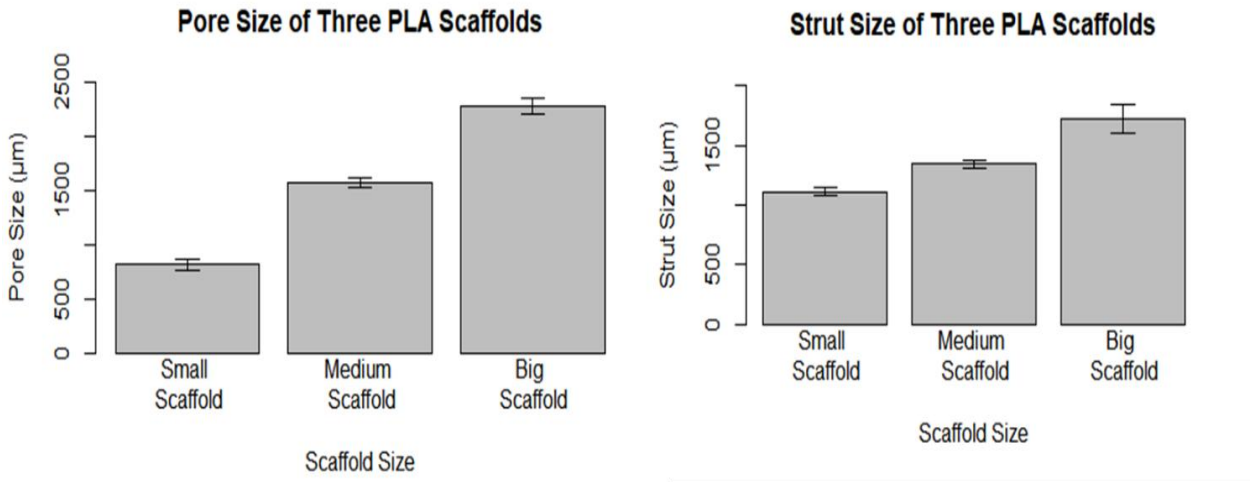

Figure 28: Strut and pore size of PLA scaffolds.

4.3.2 Deviations of Pore Size of Zinc Scaffolds from CAD model

The zinc scaffolds underwent the same macroimage analysis as the PLA scaffolds with the addition of examining the pore size distribution. The zinc scaffolds were found to have mean pore sizes of 1044.43, 1833.66, and 2383.11 µm for the small, medium, and large pore scaffolds, respectively (Table 8, Figure 29). These values are all under a 5% percent error from the CAD designs of the scaffolds. The mean

strut size for the small, medium, and large pore scaffold were 978, 1211, and 1577, respectively. Theses values also corresponded to low percent errors from the CAD designs (Table 8).

Table 8: Summary of pore size data for zinc scaffolds.

	Mean Pore Size (µm)	Stdev Pore Size (µm)	Mean Strut Size (µm)	Stdev Strut Size (µm)	% Error from CAD Specifications	
					Pore Size	Strut Size
Zinc Small Scaffold	1044.43	151.68	976.25	171.72	4.44%	2.38%
Zinc Medium Scaffold	1833.66	176.83	1211.96	231.38	4.78%	3.04%
Zinc Large Scaffold	2383.11	117.44	1577.52	64.61	4.68%	5.17%

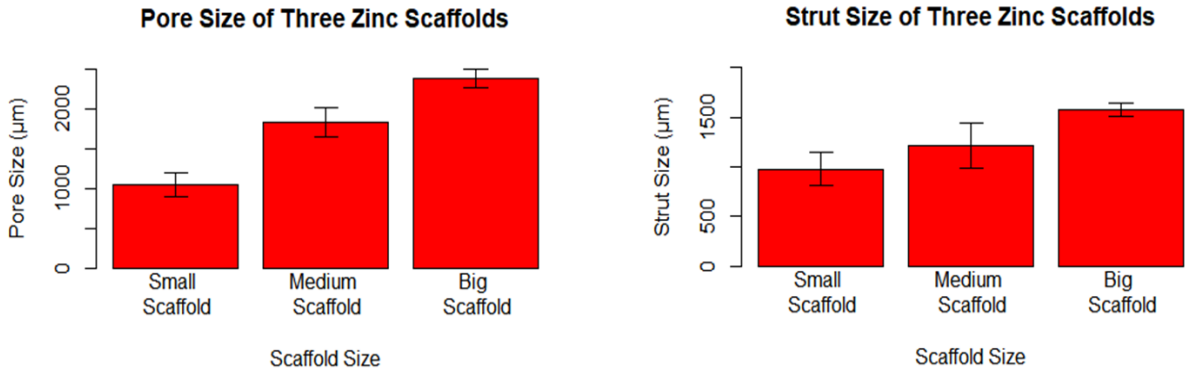

Figure 29: Pore and strut size of zinc scaffolds

The percent error for pore and strut size between the CAD/PLA and the CAD/Zinc scaffolds is significantly lower for the zinc/CAD group. This is interesting as the PLA scaffolds are the intermediate step in the process between the CAD design and the final zinc scaffold. Figure 30 shows this interesting trend where the PLA scaffold losses pore size but seems to regain it in the zinc scaffold and the vice-versa for the strut size. The reason for this is uncertain but it ends up being an advantage, allowing the final scaffold to more closely match the final structure. One explanation could be that the even during the burnout of the plastic phase, the mold undergoes heat shrinkage as it loses losses any remaining

hydration. This could lead to smaller struts and wider pores, which is the phenomena we see present in this study.

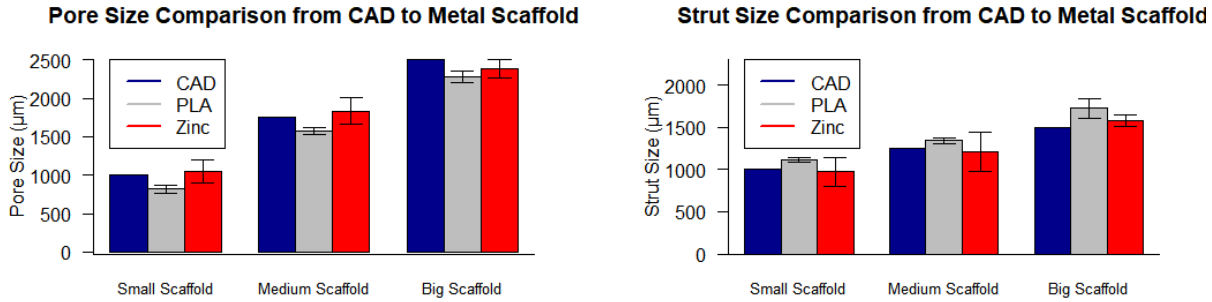

Figure 30: Side-by-Side comparison of microimaging analysis between CAD design, PLA scaffold, and Zinc scaffold.

Next, the pore size distribution is examined to determine how well the scaffolds are made to stay within the bounds of the desired pore size a scaffold should be made up of pores that are ideally identical. Figure 31 shows the distribution for the three scaffold designs for their pore size and strut size. One face of three different scaffolds was used for the pore size distribution analysis. This leads to the clear trend of the bigger pored scaffolds having a lower frequency than the smaller pored scaffolds as a big bored scaffold only had 9 pores per side while a small pored scaffold would have 56 pores per side. The

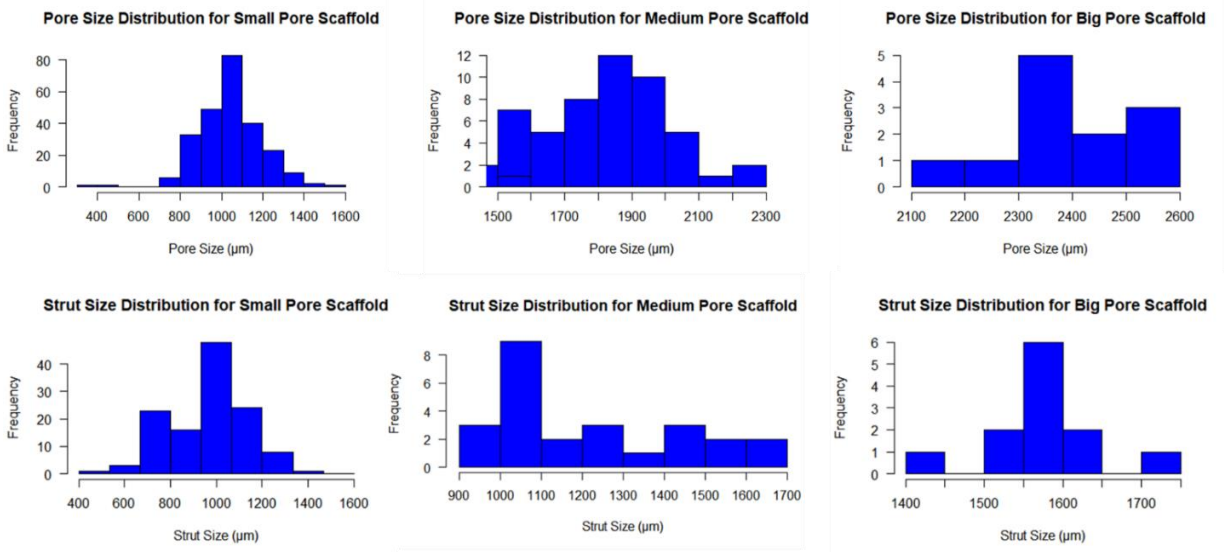

Figure 31: Pore and strut size distributions for zinc scaffolds

distributions for the small pored scaffold exhibit an expected bell curve around the mean. It is expected

that the other two samples would exhibit similar behavior given more trial. The medium pored scaffold appears to have the widest distribution of pore and strut size, but all samples keep relatively close to their CAD designs and that can be seen represented in the sample's low standard deviation in Table 8.

Figure 30 was included to show how the pore size distribution of the three scaffolds varies while viewing all samples on the same plot. Remember, the CAD designs have pore sizes of 1000, 1750, and 2500 µm. These means can be seen corresponding to their respective histograms in Figure 30. As noted earlier, in Figure 27 the pore size of the PLA scaffolds varies from pore to pore. These deviations are expected to be copied in the mold material and the final zinc scaffold.

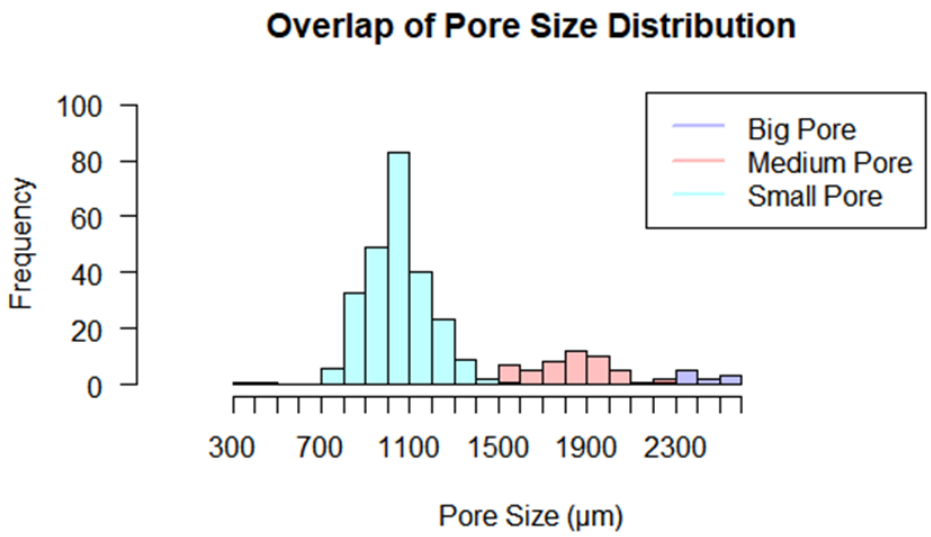

Figure 32: Graph of overlap of pore size distribution for better visualization.

4.3.3 Microimaging of Zinc Scaffolds

The scaffolds were further analyzed using SEM to look at the grains, check for different phases, and examine the micro porous structure of the scaffolds. Three SEM images are shown in Figure 33 that display the grain structure and the micro porosity of the zinc scaffolds. These images come from a

medium pored scaffold. No phase differences are seen in the images, as expected, since high purity zinc was used for the scaffold infiltration. However, micro porosity is present in these samples.

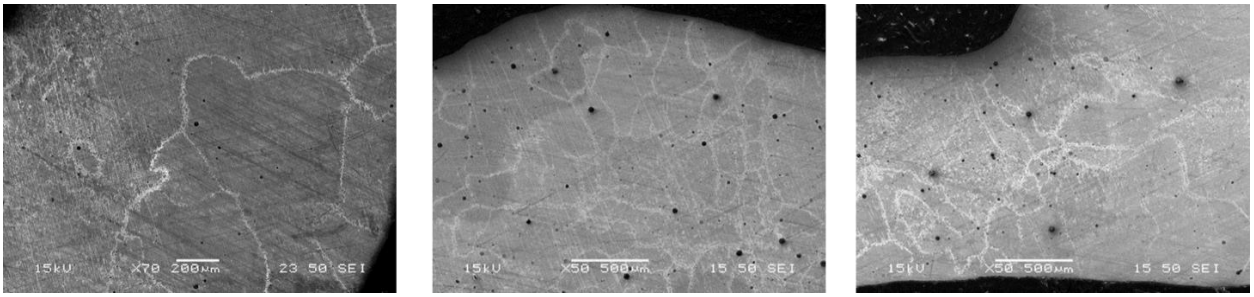

Figure 33: SEM imaging of zinc scaffolds showing grains and micro porosity.

Micro porosity has an influence on cellular properties and reactions of cells with a tissue engineering scaffolds. A certain amount of micro porosity is necessary to aid cell growth and protein interactions (Table 1). No cellular tests were performed in this thesis, but the micro porosity is still noted as it could be of use moving forward. ImageJ analysis determined the mean micropore size to be 26.17 with a standard deviation of 11.79. This high standard deviation to mean ratio can be seen in the pore size

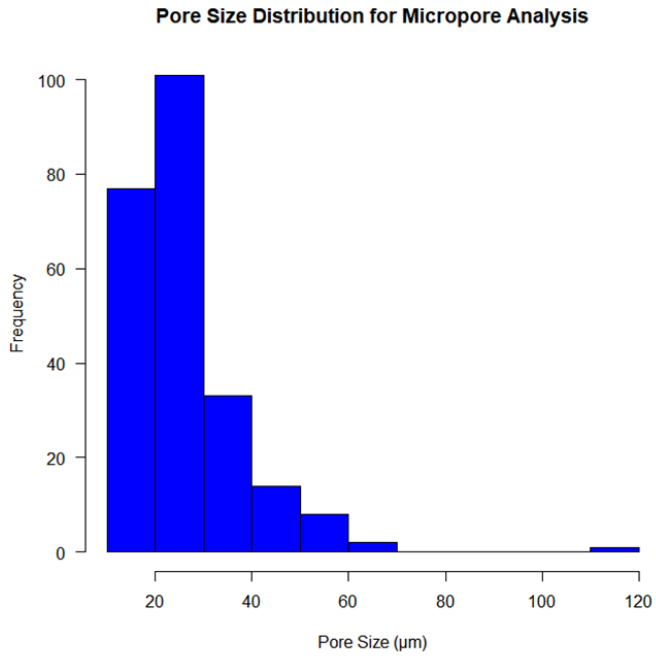

Figure 34: Micro pore size distribution for zinc scaffolds.

distribution in Figure 34. The data shows that approximately 30% of the micropores are below 20 µm which can aid in cellular attachment.

4.3.4 Mechanical Properties of Zinc Scaffolds

Compressive tests were carried out to evaluate the compression strength and stiffness of the scaffolds in relation to the three designs and to compare these properties to the mechanical properties of bone. All scaffolds were compressed between two rectangular platens in a compression device that can be seen in Figure 18. The mechanical properties such as compressive strength, stiffness, and densification were measured using the procedures described in Section 3.8. Individual graphical calculations of each calculated mechanical property can be seen in Figure 35. The summaries of the stiffness, compressive strength, and densification of the three scaffold designs are expressed in Figure 36.

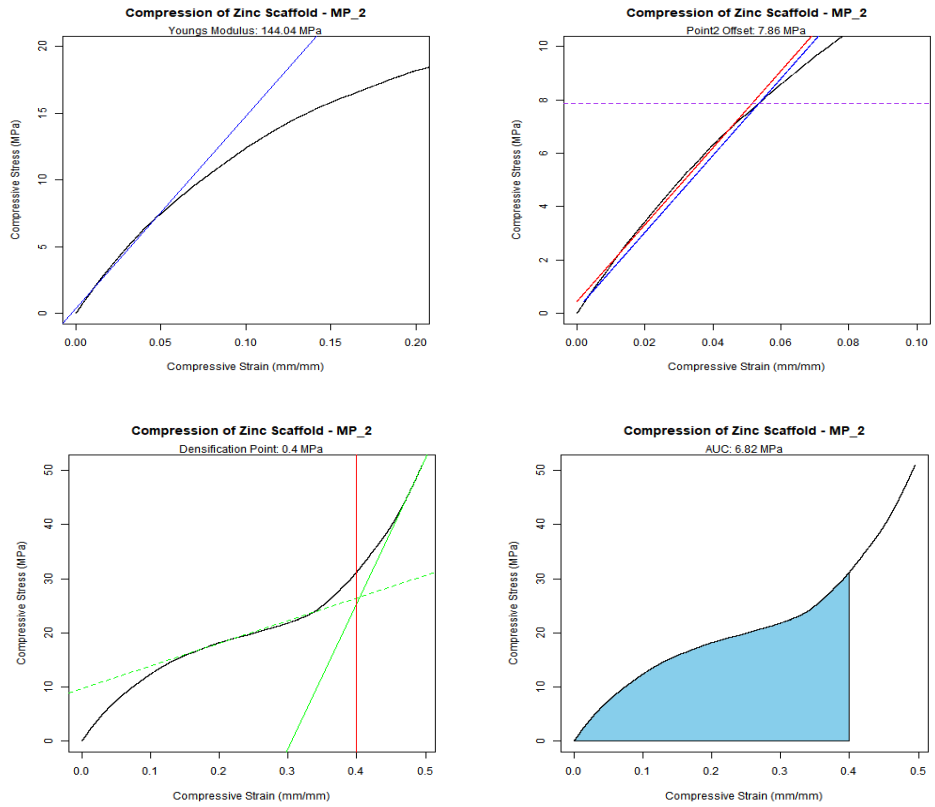

Figure 35: Graphical outputs from self created R program for the mechanical properties of a medium pored scaffold

As expected, the stiffness of the scaffolds was found to decrease with increasing pore size with the smallest pore scaffold having the highest average stiffness. Interestingly, neither the compressive strength or the densification points of the scaffolds seem to differ significantly between samples. The sample size for these trials was only n=3 so more trials could be run to confirm these results. Also, it could be that the design of the scaffolds did not vary enough to make a significant difference in these properties. Comparing the mechanical properties to bone properties in Table 8, it is found that the scaffolds compressive strength falls in the range of cancellous bone. The stiffness values of the scaffold were also found to be in the range of cancellous bone but far from that or cortical bone. The hardness of the scaffolds was 3.15 GPa with a stand deviation of 0.23 GPa. This hardness is approximately five times higher than that of human bone.

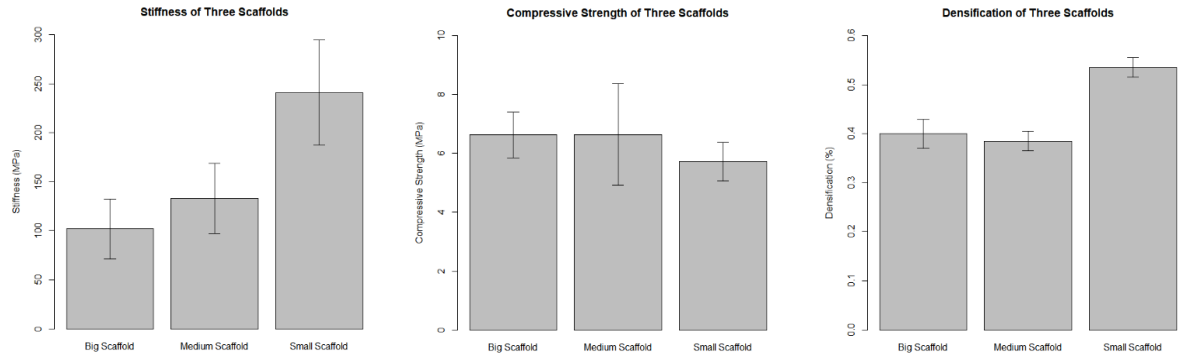

Figure 36: Mechanical Properties of three zinc scaffold designs.

CHAPTER FIVE: CONCLUSION

This research produced zinc foams that were synthesized by a new investment casting method involving the creation of multiple new mold materials. The spacer material was developed to avoid reaction between the metal and the spacer material and to be easily removed without damage to the metal foam. Additionally, the process was designed to be able to create zinc foams of varying shape and porosity and to do so safely, at a low cost, and to be able to reproduce the same design with great accuracy.

1. Zinc foams were successfully created using the new method in replicate and within 5% error of pore and strut size from their original CAD designs.
2. The process was able to produce zinc scaffolds with pore sizes varying from 1000 µm to 2500 µm.
3. The mold material was found to have little interaction with the casting process.
4. Mold material calcium sulfate was found to be easily dissolvable in a heated solution of sodium bicarbonate, which has no reaction with the metal scaffold.
5. Mechanical testing of the scaffolds showed properties like that of cancellous bone, but these properties fall short of that of compact bone.
6. Magnesium was found not to react with mold material in pressure less furnace.

5.1 Future Directions

There are several future directions that can be taken to help improve the process and test the scaffolds produced for their biomedical capabilities. While zinc is currently being explored as a metal for tissue engineering, it tends to lack the mechanical strength needed to be a proper engineering scaffold.

However, the porous zinc metal does have a current place in the biomedical field as being used for a stent. Future studies could involve designing zinc stents and producing them with this method. Additionally, an alloy using zinc and magnesium could be a promising future direction to study in conjunction with this method. The investment casting process has proven to work with zinc to produce metal scaffolds but there are still many improvements with the process that still need to be examined:

1. Determine the minimum pore and strut size or ratio of these two factors that is possible to be produced by the process. This is essential to determine how small the pore size can be that infiltration still occurs and how small the strut size can be before the mold material falls apart.
2. The calcium carbonate mold material can still be created better. Currently, some molds come out of the furnace sintered well while others show signs of cracking and flaking. Determining the optimal composition or setup to get a higher yield is desirable.
3. Determine why magnesium has a reaction in the pressure infiltrator, even when mold material and iron pipe are not present. This could be a reactor with something built into the furnace, signs of a leak letting oxygen in, or perhaps the vacuum is not strong enough.
4. Investigate how this process scales up. Specifically, the scaffolds produced here were approximately the size of a human finger bone but can they be produced at human femur size is a factor that needs to be tested and proved.

Besides the look into the future direction with these factors of the process, the scaffolds that can be produced are now ready to undergo further testing in their biological capacities:

1. Degradation testing in human body simulated fluids
2. Cell attachtment and proliferation studies
3. Cell differentiation studies on zinc and magnesium scaffolds if opted to use human stem cells as the cell type

References

[1] M. Ramalingam, Z. Haidar, and S. Ramakrishna, *Integrated biomaters for biomedical technology*. 2012.

[2] P. V. Giannoudis, H. Dinopoulos, and E. Tsiridis, "Bone substitutes: An update," *Injury*, 2005.

[3] J. M. Jukes, S. K. Both, A. Leusink, L. M. T. Sterk, C. a van Blitterswijk, and J. de Boer, "Endochondral bone tissue engineering using embryonic stem cells.," *Proc. Natl. Acad. Sci. U. S. A.*, 2008.

[4] K. Alvarez and H. Nakajima, "Metallic Scaffolds for Bone Regeneration," pp. 790–832, 2009.

[5] S. Bose, S. Vahabzadeh, and A. Bandyopadhyay, "Bone tissue engineering using 3D printing," *Materials Today*. 2013.

[6] F. Geng, L. Tan, B. Zhang, C. Wu, and Y. He, "Study on β -TCP Coated Porous Mg as a Bone Tissue Engineering Scaffold Material," vol. 25, no. 1, pp. 123–129, 2009.

[7] M. Abdel-Hady Gepreel and M. Niinomi, "Biocompatibility of Ti-alloys for long-term implantation," *Journal of the Mechanical Behavior of Biomedical Materials*. 2013.

[8] P. Erne, M. Schier, and T. J. Resink, "The road to bioabsorbable stents: Reaching clinical reality?," *CardioVascular and Interventional Radiology*. 2006.

[9] P. K. Rohatgi, N. Gupta, B. F. Schultz, and D. D. Luong, "The synthesis, compressive properties, and applications of metal matrix syntactic foams," *JOM J. Miner. Met. Mater. Soc.*, no. February, pp. 36–42, 2011.

[10] B. Jiang, C. He, N. Zhao, P. Nash, C. Shi, and Z. Wang, “Ultralight metal foams,” *Sci. Rep.*, 2015.

[11] Mahadev, C. G. Sreenivasa, and K. M. Shivakumar, “A Review on Prodution of Aluminium Metal Foams,” *IOP Conf. Ser. Mater. Sci. Eng.*, vol. 376, no. 1, 2018.

[12] J. Qin, Q. Chen, C. Yang, and Y. Huang, “Research process on property and application of metal porous materials,” *Journal of Alloys and Compounds*. 2016.

[13] F. Witte, V. Kaese, H. Haferkamp, E. Switzer, and A. Meyer-lindenberg, “In vivo corrosion of four magnesium alloys and the associated bone response,” vol. 26, pp. 3557–3563, 2005.

[14] H. Hornberger, S. Virtanen, and A. R. Boccaccini, “Biomedical coatings on magnesium alloys – A review,” *Acta Biomater.*, vol. 8, no. 7, pp. 2442–2455, 2012.

[15] X. Zhang, X.-W. Li, J.-G. Li, and X.-D. Sun, “Preparation and mechanical property of a novel 3D porous magnesium scaffold for bone tissue engineering,” *Mater. Sci. Eng. C*, 2014.

[16] E. David and H. Liu, “Investigation on magnesium degradation under fl ow versus static conditions using a novel impedance-driven fl ow apparatus,” *Prog. Nat. Sci. Mater. Int.*, vol. 24, no. 5, pp. 554–560, 2014.

[17] I. Johnson and H. Liu, “A Study on Factors Affecting the Degradation of Magnesium and a Magnesium-Yttrium Alloy for Biomedical Applications,” vol. 8, no. 6, 2013.

[18] G. Jiang and G. He, “A new approach to the fabrication of porous magnesium with well-controlled 3D pore structure for orthopedic applications,” *Mater. Sci. Eng. C*, vol. 43, pp.

317–320, 2014.

[19] N. T. Kirkland, I. Kolbeinsson, T. Woodfield, G. J. Dias, and M. P. Staiger, “Synthesis and properties of topologically ordered porous magnesium,” *Mater. Sci. Eng. B Solid-State Mater. Adv. Technol.*, vol. 176, no. 20, pp. 1666–1672, 2011.

[20] Z. S. Seyedraoufi and S. Mirdamadi, “Synthesis, microstructure and mechanical properties of porous Mg-Zn scaffolds,” *J. Mech. Behav. Biomed. Mater.*, vol. 21, pp. 1–8, 2013.

[21] S. Dutta, K. Bavya Devi, and M. Roy, “Processing and degradation behavior of porous magnesium scaffold for biomedical applications,” *Adv. Powder Technol.*, vol. 28, no. 12, pp. 3204–3212, 2017.

[22] H. Nakajima, “Fabrication, properties and application of porous metals with directional pores,” *Prog. Mater. Sci.*, vol. 52, no. 7, pp. 1091–1173, 2007.

[23] B. Arifvianto and J. Zhou, “Fabrication of Metallic Biomedical Scaffolds with the Space Holder Method: A Review,” no. ii, pp. 3588–3622, 2014.

[24] G. Kotan and a Ş. Bor, “Production and Characterization of High Porosity Ti-6A1-4V Foam by Space Holder Technique in Powder Metallurgy.,” *Turkish J. Eng. Environ. Sci.*, 2007.

[25] D. S. Li, Y. P. Zhang, X. Ma, and X. P. Zhang, “Space-holder engineered porous NiTi shape memory alloys with improved pore characteristics and mechanical properties,” *Journal of Alloys and Compounds*. 2009.

[26] O. Smorygo, A. Marukovich, V. Mikutski, A. A. Gokhale, G. J. Reddy, and J. V. Kumar, “High-porosity titanium foams by powder coated space holder compaction method,”

Mater. Lett., 2012.

[27] I. Gligor *et al.*, “Porous c.p. titanium using dextrin as space holder for endosseous implants,” *Part. Sci. Technol.*, 2013.

[28] S. W. Kim, H. Do Jung, M. H. Kang, H. E. Kim, Y. H. Koh, and Y. Estrin, “Fabrication of porous titanium scaffold with controlled porous structure and net-shape using magnesium as spacer,” *Mater. Sci. Eng. C*, 2013.

[29] P. J. Kwok, S. M. Oppenheimer, and D. C. Dunand, “Porous titanium by electro-chemical dissolution of steel space-holders,” *Adv. Eng. Mater.*, 2008.

[30] V. Karageorgiou and D. Kaplan, “Porosity of 3D biomaterial scaffolds and osteogenesis,” *Biomaterials*. 2005.

[31] Y. Li *et al.*, “Additively manufactured biodegradable porous magnesium,” *Acta Biomater.*, vol. 67, pp. 378–392, 2018.

[32] L. Zhao *et al.*, “Mechanical properties and in vitro biodegradation of newly developed porous Zn scaffolds for biomedical applications,” *Mater. Des.*, vol. 108, pp. 136–144, 2016.

[33] J. Čapek, E. Jablonská, J. Lipov, T. F. Kubatík, and D. Vojtěch, “Preparation and characterization of porous zinc prepared by spark plasma sintering as a material for biodegradable scaffolds,” *Mater. Chem. Phys.*, vol. 203, pp. 249–258, 2018.

[34] Y. Hou *et al.*, “Synthesis of biodegradable Zn-based scaffolds using NaCl templates: Relationship between porosity, compressive properties and degradation behavior,” *Mater. Charact.*, vol. 137, no. November 2017, pp. 162–169, 2018.

[35] J. Malda *et al.*, “Oxygen Gradients in Tissue-Engineered PEGT/PBT Cartilaginous Constructs: Measurement and Modeling,” *Biotechnol. Bioeng.*, 2004.

[36] K. Rezwan, Q. Z. Chen, J. J. Blaker, and A. R. Boccaccini, “Biodegradable and bioactive porous polymer/inorganic composite scaffolds for bone tissue engineering,” *Biomaterials*. 2006.

[37] D. R. Sumner, T. M. Turner, R. Igloria, R. M. Urban, and J. O. Galante, “Functional adaptation and ingrowth of bone vary as a function of hip implant stiffness,” vol. 31, 1998.

[38] S. Gallinetti, “New Approaches in Calcium Phosphate Cements and Ceramics for Bone Regeneration,” 2014.

[39] K. Rezwan, Q. Z. Chen, J. J. Blaker, and A. Roberto, “Biodegradable and bioactive porous polymer / inorganic composite scaffolds for bone tissue engineering,” vol. 27, pp. 3413–3431, 2006.

[40] Y. H. An and R. a. Draughn, “Mechanical Testing of Bone and the Bone-Implant Interface,” *Medical*, 1999.

[41] E. D. Mcbride, “Absorbable metal in bone surgery: A FURTHER REPORT ON THE USE OF MAGNESIUM ALLOYS,” *J. Am. Med. Assoc.*, 1938.

[42] M. Niinomi, M. Nakai, and J. Hieda, “Development of new metallic alloys for biomedical applications,” *Acta Biomaterialia*. 2012.

[43] G. Song, “Recent Progress in Corrosion and Protection of Magnesium Alloys,” *Adv. Eng. Mater.*, 2005.

[44] H. Zhuang, Y. Han, and A. Feng, “Preparation , mechanical properties and in vitro biodegradation of porous magnesium scaffolds,” *Mater. Sci. Eng. C*, vol. 28, no. 8, pp. 1462–1466, 2008.

[45] M. Yazdimamaghani, M. Razavi, D. Vashaee, K. Moharamzadeh, A. R. Boccaccini, and L. Tayebi, “Porous magnesium-based scaffolds for tissue engineering,” *Mater. Sci. Eng. C*, vol. 71, pp. 1253–1266, 2017.

[46] J. Zhang *et al.*, “Influence of fluoride treatment on surface properties, biodegradation and cytocompatibility of Mg-Nd-Zn-Zr alloy,” *J. Mater. Sci. Mater. Med.*, 2014.

[47] M. Cheng, T. Wahafu, G. Jiang, W. Liu, and Y. Qiao, “A novel open-porous magnesium scaffold with controllable microstructures and properties for bone regeneration,” *Nat. Publ. Gr.*, no. April, pp. 1–14, 2016.

[48] L. Pan *et al.*, “Fluoride promotes osteoblastic differentiation through canonical Wnt/β-catenin signaling pathway,” *Toxicol. Lett.*, 2014.

[49] G. Hannink and J. J. C. Arts, “Bioresorbability , porosity and mechanical strength of bone substitutes : What is optimal for bone regeneration ?,” *Injury*, vol. 42, pp. S22–S25, 2011.

[50] J. Kemppainen, “Mechanically stable solid freeform fabricated scaffolds with permeability optimized for cartilage tissue engineering,” 2008.

[51] L. G. Sicchieri, G. E. Crippa, P. T. de Oliveira, M. M. Beloti, and A. L. Rosa, “Pore size regulates cell and tissue interactions with PLGA-CaP scaffolds used for bone engineering,” *J. Tissue Eng. Regen. Med.*, 2012.

[52] N. Gupta and P. Rohatgi, *Metal matrix syntactic foams: processing, microstrucutre,*

properties, and applications. DEStech Publications, 2014.

[53] S. Sánchez-Salcedo, D. Arcos, and M. Vallet-Regí, "Upgrading Calcium Phosphate Scaffolds for Tissue Engineering Applications," *Key Eng. Mater.*, vol. 377, no. March, pp. 19–42, 2009.

[54] Y. Chien, C. Liang, S. Liu, S. Yang, and Y. Chien, "Combustion Kinetics and Emission Characteristics of Polycyclic Aromatic Hydrocarbons from Polylactic Acid Combustion Combustion Kinetics and Emission Characteristics of Polycyclic Aromatic Hydrocarbons from Polylactic Acid Combustion," *J. Air Waste Manag. Assoc.*, vol. 2247, 2012.

[55] M. Doube, M. M. Kłosowski, I. Arganda-carreras, and P. Fabrice, "UKPMC Funders Group BoneJ : free and extensible bone image analysis in ImageJ," *Bone*, vol. 47, no. 6, pp. 1076–1079, 2010.

[56] M. Haeri and M. Haeri, "ImageJ Plugin for Analysis of Porous Scaffolds used in Tissue Engineering," *J. Open Res. Softw.*, vol. 3, pp. 2–5, 2015.

[57] P. Feng, P. Wei, C. Shuai, and S. Peng, "Characterization of mechanical and biological properties of 3-D scaffolds reinforced with zinc oxide for bone tissue engineering," *PLoS One*, vol. 9, no. 1, 2014.